2020

The Effects of Carbon Equivalent, Return Ratios, Mold Preparation, Riser Feed and Casting Temperature on the Microstructural and Mechanical Properties of 100-70-03 Pearlitic Ductile Iron

Erin VanDusen

THE EFFECTS OF CARBON EQUIVALENT, RETURN RATIOS, MOLD PREPARATION, RISER FEED AND CASTING TEMPERATURE ON THE MICROSTRUCTURAL AND MECHANICAL PROPERTIES OF 100-70-03 PEARLITIC DUCTILE IRON

By

Erin VanDusen

A THESIS

Submitted in partial fulfillment of the requirements for the degree of

MASTER OF SCIENCE

In Materials Science and Engineering

MICHIGAN TECHNOLOGICAL UNIVERSITY

2020

This thesis has been approved in partial fulfillment of the requirements for the Degree of MASTER OF SCIENCE in Materials Science and Engineering.

Department of Materials Science and Engineering

Thesis Advisor:	*Paul Sanders*
Committee Member:	*Joseph Licavoli*
Committee Member:	*Douglas Swenson*
Department Chair:	*Stephen Kampe*

Table of Contents

Acknowledgements

Thank you to my advisor, Dr. Paul Sanders for helping find a project to suit my interests, expanding my professional network, and guiding me through my research.

This project would not have been possible without the guidance and financial support given by Jiten Shah and Product Development and Analysis as well as Frank Headington and the American Foundry Society.

My sincere appreciation is extended to:

The foundry staff at Michigan Technological University: Dr. Dale Dewald, Russ Stein, Dr. Joseph Licavoli, and Tom Wood. The foundry undergraduate team: Alex Basaj, Nick Martin, and Isabella Wakeham. Thank you for all your assistance in experimentation, on the fly thinking, and heavy lifting.

The team that helped me find flasks and jackets: Greg Miskinis of Waupaca Foundry, Tom Gaeding and Mike Kamin of Carpenter Brothers, Inc., and Grant Wightman and Ben Svoboda of Winnebago Foundry. I am grateful for your kindness, generosity, and resourcefulness.

Brian Began, TJ Gaines, and Abhay Pande at Foseco Int. Ltd. (Vesuvius USA) for the riser sleeve and filter donations and their generous contribution of time and knowledge.

Mike Riabov and Elkem for their desire to facilitate research and education with the donation of inoculation and alloying materials.

Lizeth Medina, for being a mentor, and the technical services team, John Falecki and Ryan Spaulding, at Neenah Foundry Co. for analysis, tensile bar fabrication, and testing.

Thank you to my MSE family, Ale Almanza, Matt Thomas, and Mike Sulwer for support, a helping hand, and wonderful friendships. There is no chance that we will ever forget each other.

Thank you to my wonderful parents who have always supported me and believed in me. Merci beaucoup.

Abstract

The most common and costly detriments to ductile iron foundries are casting defects, particularly in new and complex components. The ability to understand the factors and processes that create microstructures and the associated properties would allow accurate virtual predictions of casting outcomes. An experimental study of standard foundry variables, carbon equivalent, return ratio, mold preparation, riser feed, and casting temperature on a target of 100-70-03 pearlitic, hypereutectic ductile iron provided the groundwork for an ICME database. Density decreased when the fraction of graphite nodules was greater due to the low density of graphite. A greater percentage of return scrap and higher CE level correlated to increased graphite nodule formation and count as well as increased hardness and density. Riser sleeve compression and mold hardness influenced the amount of material fed into a casting upon solidification. However, mold hardness in the range of 85 to 95 B-scale has little effect on the microstructure and mechanical properties of the casting.

1 Introduction and Background

1.1 Ductile Iron Overview

Ductile iron, which is typically cast, is a versatile material with exceptional strength and toughness that make it ideal for applications in the automotive, agricultural machinery, pipe, construction, and defense industries. Since ductile iron is often used in critical components, the quality of the casting is imperative. Foundries have been implementing component and casting simulation modeling software to predict the final casting properties of components, however there is a need to improve the accuracy of predictions to reduce time and cost related to casting defects or inadequacies. Porosity, sand inclusions, and other potentially avoidable defects cost the foundry industry millions of dollars a year from scrapped parts and repeating jobs. For example, links between sand properties and microstructure can be used to estimate density and predict porosity. The ability to prevent these defects not only reduces scrap and re-working, but it cuts job time requirements in half.

1.2 Ductile Iron and ICME

Current predictive methods applied in ductile iron foundries involve modeling a component then assessing the casting outcome in a casting simulation software. Although useful, there are not extensive databases nor exceptionally accurate software for predicting specific microstructural details and properties. Taking this further, the integrated computational materials engineering (ICME) approach encompasses a wide variety of simulation technology to comprehensively model the microstructure and resulting properties of materials. This methodology allows extensive virtual component design, testing, and optimization before physical fabrication occurs. This is done by simulating known interactions between the microstructure and properties of a given material to the design in question with multilevel simulation tools. This strategy minimizes the time and costs of component design, development, and integration into mass production [1].

Experimental results from metallurgical and mechanical testing of 100-70-03 grade hypereutectic pearlitic ductile iron examined under a variety of casting conditions were

accumulated and analyzed to lay the groundwork for an ICME database. The experimental data was analyzed for statistically significant correlations between carbon equivalent, return scrap percentage, mold preparation, riser feed, and casting temperature on the microscopy, density, hardness, and tensile properties of the final casting.

1.3 The Structure of Ductile Iron

Ductile iron with a tensile strength of 100 psi, a yield strength of 70 psi, and an elongation of 3% (100-70-03 grade) is a common grade for critical components, such as crank shafts, that require high strength but need some elongation to prevent brittle fracture. The mechanical properties of any materials are determined primarily by the microstructure, which in ductile iron, is comprised of ferrite, pearlite, and graphite nodules (Figure 1).

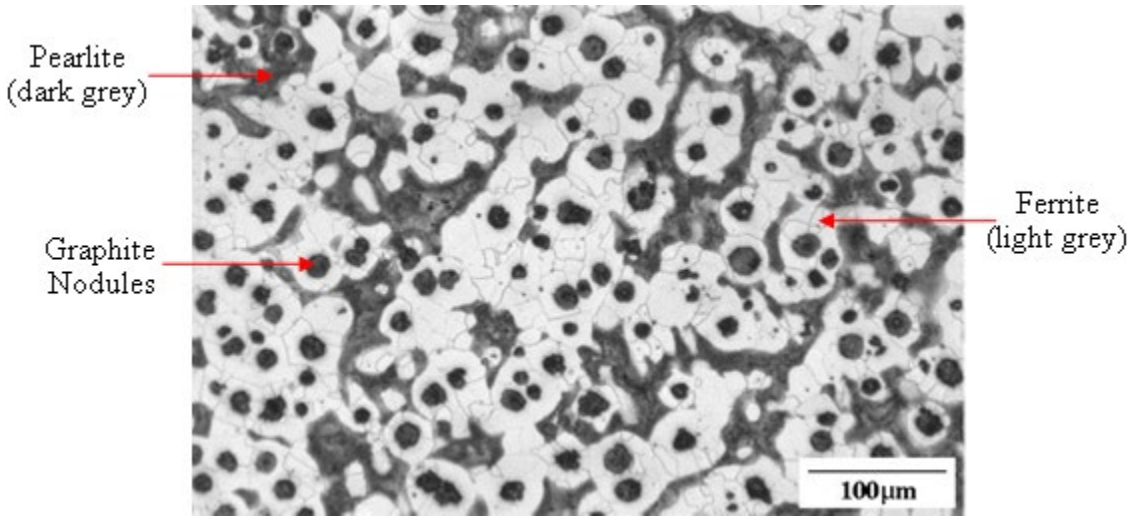

Figure 1. Ductile iron micrograph [2].

Ferrite refers to iron in a body-centered cubic crystal structure with a density of 0.282 lb/in³ (7.81 g/ cm³) [3], and is a matrix component. Since ferrite is softer and more deformable, it provides the elongation to ductile iron. Pearlite is a combination of ferrite and the iron carbide, cementite (Fe_3C) in a lamellar structure with a density of 0.277 lb/in³ (7.67 g/cm³) [4]. Pearlite is stronger than ferrite, and thus provides increased alloy strength but sacrifices elongation. The graphite nodules are spherical and have a low density of 0.081 lb/in³ (2.23 g/cm³) [5] and a low hardness. The combination of these

microconstituents provides the exemplary toughness of ductile iron compared to grey cast iron which is stronger, but more brittle, due to its continuous graphite flake microstructure.

1.4 Alloying Elements

1.4.1 Eutectic Point and Carbon Equivalent

The iron-carbon system is well known in the field of metallurgy. A general prediction of ductile iron phases can be made using the metastable iron-carbon phase diagram *Figure 2*). The eutectic point of 4.3 wt.% carbon distinguishes the point at which the liquid freezes into two solid phases. A hypereutectic composition promotes graphite formation and reduces chill [6].

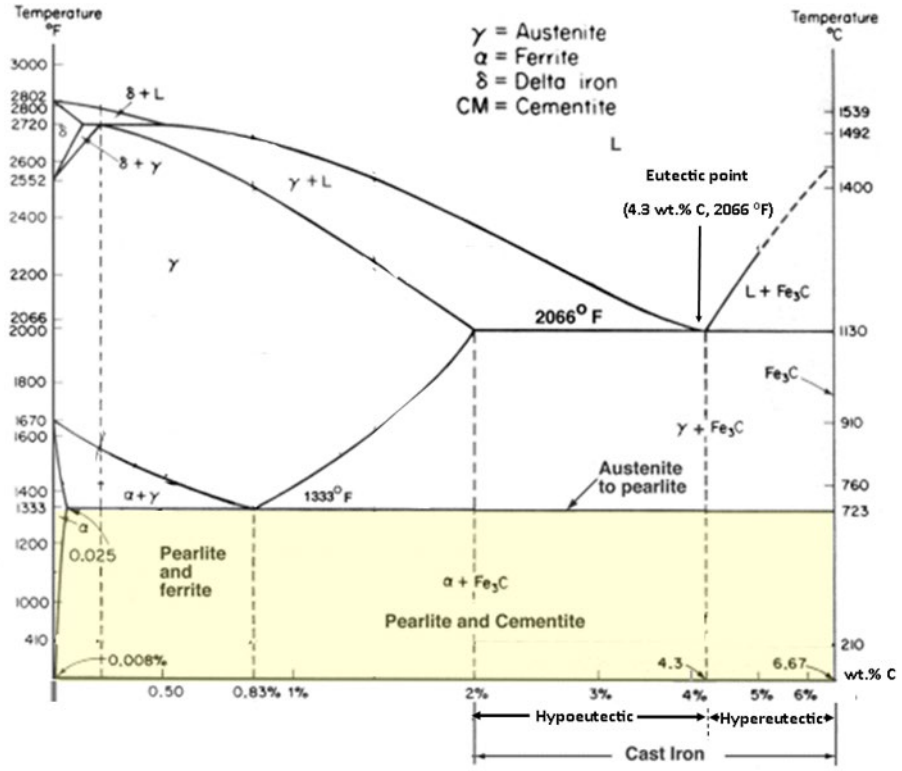

Figure 2. Metastable Iron-Carbon Phase Diagram with the regions of interest highlighted [2].

Silicon increases the influence of carbon in ductile iron and promotes graphite formation over carbides. Their combined graphitizing power is the carbon equivalent (CE) which

can be calculated, it the simplest form, by Equation 1 with all elements measured in wt.%.

$$CE = C + \frac{1}{3}Si \quad \text{Eq. 1}$$

Other elements that can noticeably influence CE are phosphorus and manganese. A CE that is too high has negative consequences such as exploded graphite formation, graphite clustering, and graphite flotation [6]. These forms of graphite are detrimental to mechanical properties. A CE that is too low will not form the nodular structure.

1.4.2 Copper

The microstructure for a 100-70-03 grade ductile iron contains a higher ratio of pearlite to ferrite. This microstructure can be obtained with a variety of casting conditions. The most common method of obtaining approximately 80% pearlite involves increased alloying additions of copper or tin. Additions of copper, in particular, promote pearlite formation without increasing the tendency of carbide formation which would increase the brittleness of the alloy [7].

Varying section thicknesses in a casting have various cooling rates that influence the microstructure. Since ferrite formation is promoted in slower cooling (thicker) sections, compared to pearlite in thinner sections, the microstructure can be heterogenous across the casting. Copper can equilibrate the entire component microstructure to be fully pearlitic by varying the alloying range. Commonly, ductile iron contains a range of 0.1 wt.% to 0.6 wt.% copper, depending on the section thickness variation in the casting. A higher copper content results in a more pearlitic microstructure.

1.4.3 Charge Material

The constitution of the charge material plays an important role in the chemistry and microstructure of the resulting ductile iron casting. Typically, the iron-based charge material is made up of steel scrap, pig iron, and foundry returns in a ratio that satisfies not only chemistry requirements, but microstructural needs as well. Overall, phosphorous and sulfur content must be restricted for ductile iron because phosphorous lowers ductility and sulfur reacts with magnesium. This reaction reduces the effectiveness of the

magnesium treatment which effects nodularity. Also, higher sulfur contents can generate sulfide inclusions that weaken the casting [7].

Steel scrap is desirable due to the low cost and low phosphorous and sulfur content. However, the quality and variety of steel scrap can vary greatly, which will impact the ductile iron casting. Processed scrap, such as bushelling, is more expensive, but more reliable scrap because the chemistry range is known. On the other hand, obsolete scrap, such as engine blocks, machinery scrap, and bridge scrap, is less dependable. The chemistry varies significantly across scrap from various applications. Often, the manganese content of obsolete is too high for primarily ferritic grades [7].

The most reliable and preferred charge material for ductile iron is pig iron. Pig iron is a crude iron tapped from a blast furnace and cast into ingots for use in steel and cast iron. It is over 90 wt.% iron and has a high carbon content with low phosphorous, manganese, and sulfur content. Pig iron can make inoculation easier because it contains residual nuclei [7]. The disadvantage of pig iron is the cost. It is expensive because of the low trace elements and the known composition.

Foundry return scrap is comprised of gating and runner systems, risers, and any defective castings that were scrapped. Return scrap is beneficial because the chemistry is known and desired. Additionally, for ductile iron, any nodule nuclei can make inoculation easier. Typically, alloys of vastly different chemistries and microstructures are not mixed, such as grey iron and ductile iron or two ductile irons with varying silicon levels. Return scrap is a necessary byproduct of the casting process, therefore it is cost effective to use it as charge material at approximately the rate it is produced. The price of the return scrap is seen in the cost of energy from re-melting, rather than material cost. The ideal combination of charge materials balances cost and chemistry to produce a quality casting at a reasonable price.

1.5 Collapsible Riser Sleeves

Risers are a common practice to ensure the soundness of castings. They function by remaining molten as the casting is solidifying and feed the casting through the neck to fill

any regions of shrink. There has been a great deal of research and experimentation to select appropriate riser sizes that counter shrink without producing excessive return scrap. Riser sleeves aid in reducing scrap by insulating risers. This is taken a step further with exothermic riser sleeves that further extend the time that the riser feeds the casting by producing heat from a chemical reaction.

Some riser sleeves have a collapsible metal breaker core (Figure 3). This creates a customizable neck length on the riser to allow spot feeding and to improve sand compaction beneath the sleeve since it is compressed during molding.

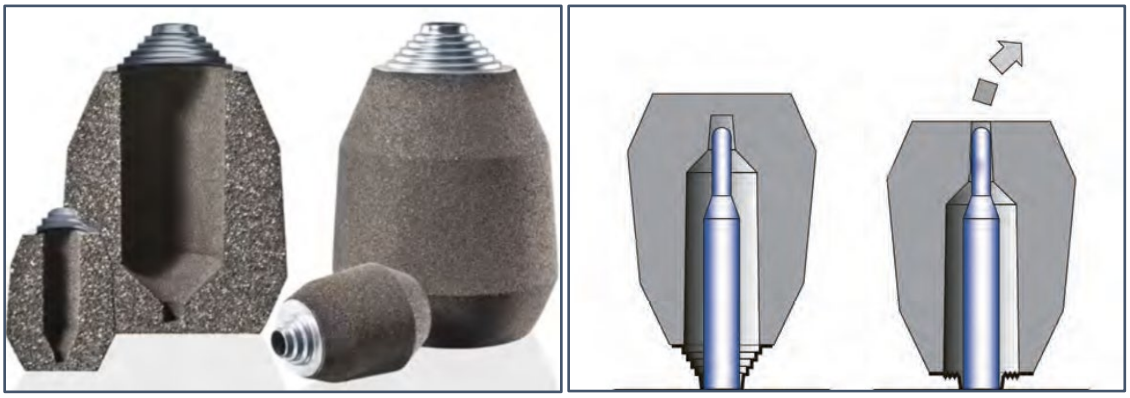

Figure 3. (a) FEEDEX K riser sleeves with collapsible metal breaker core (Foseco International Ltd.) (b) Riser sleeve cartoon depicting the compression of the metal core during molding [8].

The benefits of the steel breaker core include improved strength, the ability to compact under higher pressure molding processes. Additionally, there is a decreased chance of loose insulating material tumbling into the riser neck and subsequently contaminating the casting, and a mitigated risk of graphite degeneration from contact with exothermic material [8]. Since the insulating, exothermic riser sleeve is more efficient, the contact area with the casting is only 2.8% that of a traditional sand riser. Although exothermic riser sleeves are more expensive that sand risers or only insulating sleeves, they reduce fettling costs significantly.

1.6 Hypothesis

If the carbon equivalent and return scrap ratio are increased, then the casting density will decrease because graphite nodules, which have a lower density, will be able to nucleate more easily and rapidly, thereby allowing carbon to diffuse to growing graphite nodules instead of forming cementite in pearlite.

2 Experimental Methods

2.1 Modeling

A test plate casting was designed to imitate a production part with a green sand mold and a chemically bonded core. A 12x12.75x1 inch plate was designed in SOLIDWORKS modeling software with a centered riser surrounded by an exothermic riser sleeve in the green sand cope and a chemically bonded drag (Figure 4). The gate fed the casting along the bottom of a 12.25-inch edge and a choke regulated the flow. The gate was 1-inch from the pouring basin on the 5.3-inch runner to form a sand trap. A filter adjacent to the sprue well removed impurities from iron before it entered the runner.

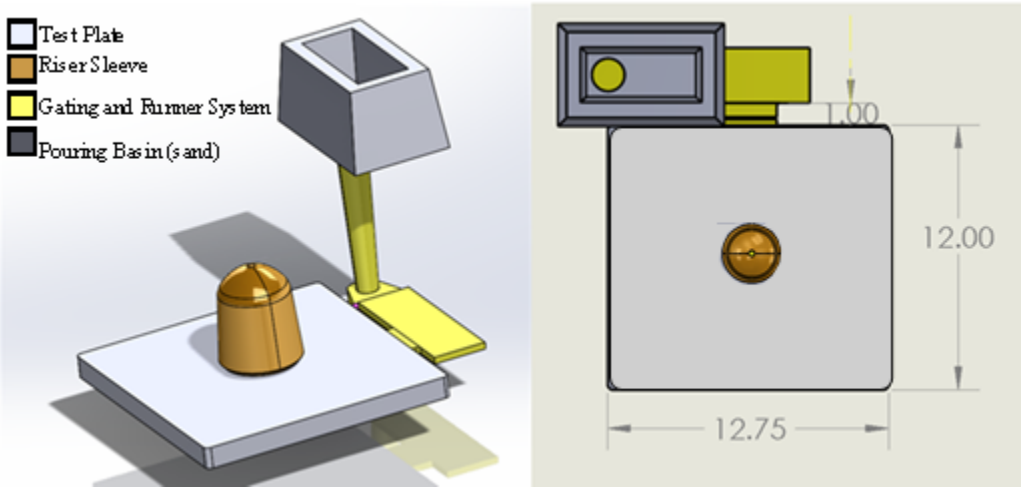

Figure 4.Test plate model created in SOLIDWORKS.

Predictive casting modeling was performed by Jiten Shah (Product Development and Analysis LLC) using MAGMA software. A mold size of 16x20x6” with a 1” upset on the cope was added to the model and the riser sleeve was indicated to be the insulating ASK/US_EXF_EXACTCAST riser sleeve from the MAGMA iron database. Predictive porosity and flow modeling was done with the following parameters: a 10 ppi foam filter,

an initial mold temperature of 25°C, and a pour temperature of 1400°C (Figure 5). The models predicted sound castings with sufficient metal flow rates and patterns.

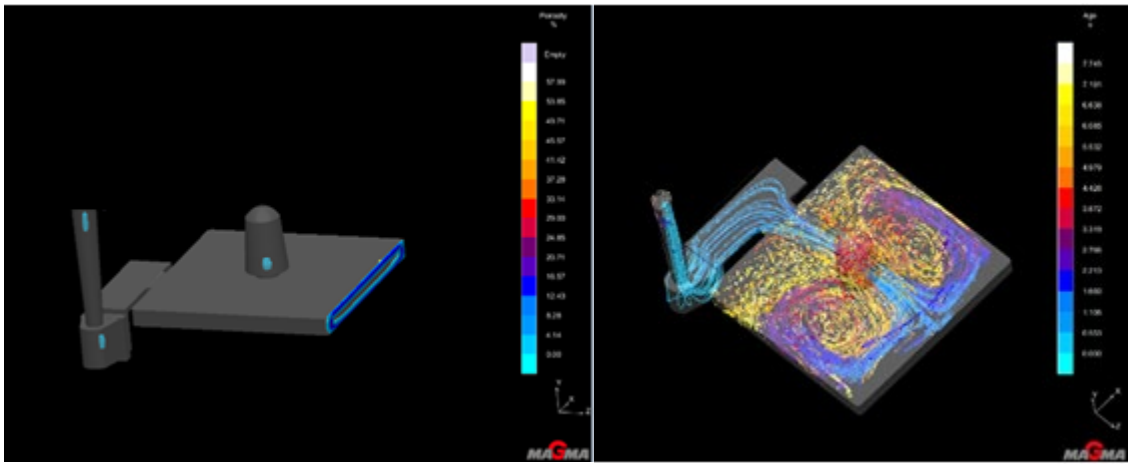

Figure 5. Test plate porosity and metal flow predictions from MAGMA software.

2.2 Design of Experiments

A design of experiment (DOE) was carried out in four heats producing four castings each. The carbon equivalent (CE) was investigated at two levels: 4.35, slightly above the eutectic point, and 4.60, a higher value for ductile iron.

The pouring temperatures were set to 2500 and 2600 °F. 2500 °F is a low pouring temperature for ductile iron and can run the risk of causing defects if the magnesium treatment is not properly carried out. 2600 °F is similar to the industry standard for ductile iron.

Green sand mold hardness was studied at levels of 85 and 95 on the B-scale. This scale measures hardness by determining how much the surface in question can compact under the indenter. Less compaction designates a harder green sand mold. For an industrial squeeze press molding machine, the sand hardness levels lie within the 85-95 range.

Simultaneously, the percentage of returns in the furnace charge was varied between 40% and 60%. Typically, return scrap is consumed at approximately the rate it is produced, which is determined by the casting yield. Although many components have better yield and produce less than 60% scrap, the extreme case was investigated.

Using Minitab software, a half-fraction DOE was constructed which consisted of 16 castings (Table 1). This was a resolution IV design with confounded two-factor and three-way interactions. Although not a part of the DOE, the pour time for each mold was recorded to track consistency.

Table 1. Design of experiments summary for responses of microscopy, density, hardness, strength, and elongation

Run Number	Sleeve Compression (%)	Mold Hardness (B-Scale)	CE	Pour Temperature (°F)	Charge Returns (%)
1	70	95	4.35	2500	40
2	100	85	4.35	2500	40
3	70	85	4.35	2600	40
4	100	95	4.35	2600	40
5	70	85	4.60	2500	40
6	100	95	4.60	2500	40
7	70	95	4.60	2600	40
8	100	85	4.60	2600	40
9	70	85	4.35	2500	60
10	100	95	4.35	2500	60
11	70	95	4.35	2600	60
12	100	85	4.35	2600	60
13	70	95	4.60	2500	60
14	100	85	4.60	2500	60
15	70	85	4.60	2600	60
16	100	95	4.60	2600	60

The riser sleeves used were Kalminex 2000XP K226 exothermic riser sleeves (Foseco International Ltd.) with a 1” diameter collapsible neck (Figure 6). The riser sleeves were pre-crushed to levels of 70% and 100% neck compression by height using a Black Widow 20-ton shop press (Discount Ramps).

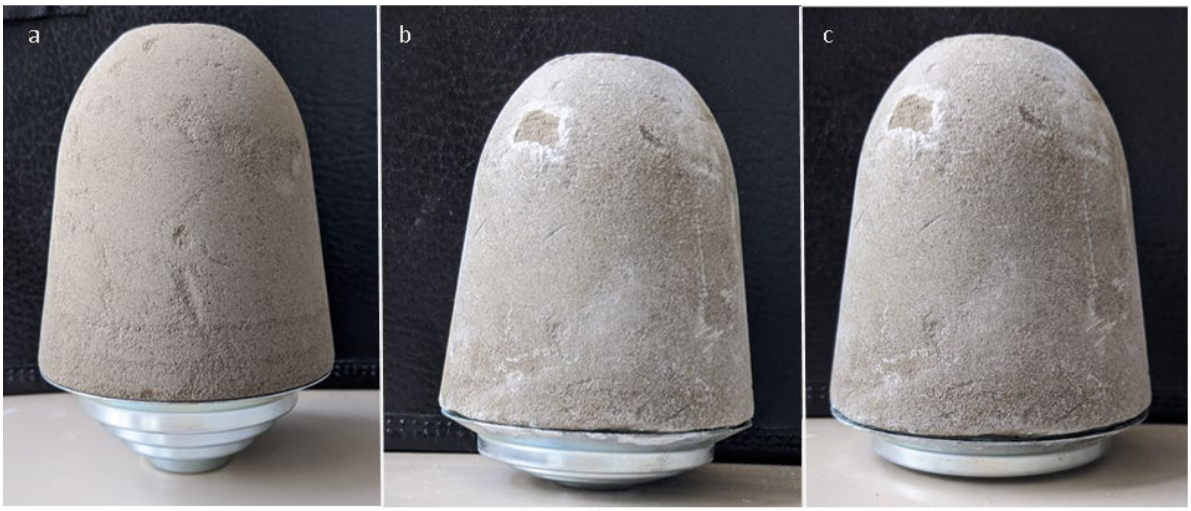

Figure 6. Foseco Kalminex 2000XP K226 Exothermic Collapsible Riser Sleeve (a) uncompressed, (b) 70% compression, and (c) 100% compression.

2.3 Casting

2.3.1 Molding

The test plate pattern was constructed from wood with a 2-degree draft, secured with wood glue and screws, then coated in a clear polyurethane wood finish. The drag was made of a two-part alkaline phenolic, no-bake chemically bonded sand mixed in a Tinker Omega TOM-125. The chemically bonded sand contained 1.25% ALPHASET 9010 resin and 30% ALPHACURE 110 catalyst (HA International, LLC). Each drag was approximately 100 lbs. and was left to cure for 15 minutes before removing the pattern. All drags were left in ambient air for approximately 24 hours before the pour. The full chemically bonded sand molding SOP is located in Appendix C.

The cope was made from green sand mixed in a Mix-Muller (Simpson Technologies) to approximately 55% compactibility. With the drag placed in the flask, a dusting of parting compound was applied to the pattern and a layer of riddled sand was gently rammed around the pattern and under the riser sleeve. A ¼ inch diameter rod was inserted into each sleeve to create a vent in the top of each riser and through the green sand. Another layer of sand was packed down and rammed using a pneumatic rammer. This was repeated until the flask was full. The remaining sand was struck off to create a level surface, a small well was dug around the venting rod and the venting rod was removed.

The mold was moved to the 20-ton shop press and a press plate was placed on top. Pressure was applied until the surface hardness was measures to be 85 or 95 on the B-scale, according to the DOE, using an Electronic Green Hardness (Tester Simpson Technologies).

After pressing, a 1-inch top diameter and ½ inch base diameter sprue was cut into the green sand and a larger well was formed around the vent to capture the overflow. The pattern was removed, and a 10 ppi SEDEX 66x66x13mm ceramic filter (Foseco) was placed in the filter print of the drag. The mold was re-assembled, and the flask removed. After placing a jacket around the mold parting line, a chemically bonded pouring basin was positioned on top and secured with green sand. The mold was clamped to avoid cope lift and subsequent breakouts at the parting line.

2.3.2 Chemistry and Casting

Four molds were made and poured per heat. The charge consisted of either 40 or 60% ductile iron returns in approximately a 250 lb. heat, according to the DOE, with the remainder containing steel punchings, pig iron, and various alloying additions (Table 2).

Table 2. Iron charge material breakdown for 40 and 60% return scrap in a 250 lb. heat.

Charge Material	Content for 40% return scrap (%)	Content for 60% return scrap (%)
Return Scrap	30	20
Pig Iron	30	20
Steel punchings	40	60

The copper content was 0.90 wt.% to ensure a pearlitic microstructure. Additionally, carbon was added in the form of Desulco 9001, the silicon was added in the form of 75%FeSi (Elkem) and the manganese was in the form of FeMn (Hickman-Williams). The carbon and silicon contents for each CE factor of the DOE were broken up as shown in Table 3.

Table 3. Carbon and silicon levels comprising the DOE CE factors.

CE	C (wt.%)	Si (wt.%)
4.35	3.75	1.80
4.60	3.80	2.40

A 300 lb. capacity tundish ladle was preheated and just before tapping the furnace, the MgFeSi (Hickman-Williams) and ladle treatment of cover steel and Topseed (Elkem) were inserted via the sandwich method (steel covering the MgFeSi) into the tundish before the lid was situated. The furnace was tapped into the spout of the ladle with the inoculation added in-stream. The inoculation consisted of Elkem Reseed (1-3 mm). The Mg reaction was allowed to finish before pouring. The first two molds were poured at approximately 2600°F, then a spectral button was poured, the temperature was measured, and the second two molds were poured at approximately 2500°F. Each mold was filled until iron flowed out of the riser vent. The test plates were broken out of the molds approximately 12 hours after pouring.

2.3.3 Sectioning

Excess sand on the surface was removed by sand blasting the test plates. The sprue, sprue well, and runner were removed with an angle grinder then recycled as returns.

The test plate was then sectioned (Figure 7) for microscopy, density, strength, and hardness characterization using a Bayleigh Industrial band saw. The area beneath the riser (sub-riser section) was selected for density measurements because that is where porosity would be expected according to the MAGMA model.

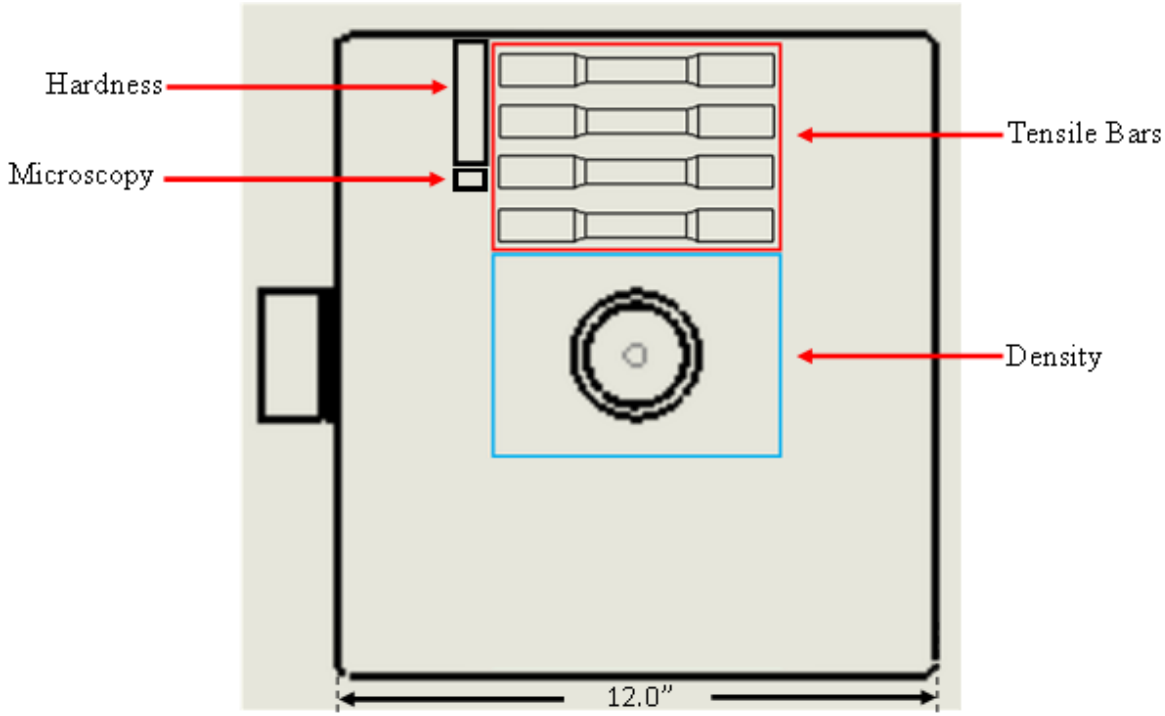

Figure 7. Diagram of test plate sectioning for characterization.

2.4 Polishing and Microscopy

Each microscopy specimen was manually ground with Buehler SiC grinding discs and 6 µm, 3 µm, and 1 µm polycrystalline diamond compounds with propylene glycol-based lubricant, RedLube (Allied High Tech Products, Inc.), according to the steps in Table 4. The final polish was a 0.05 µm alumina suspension.

Table 4. Ductile iron polishing steps

Polishing Step	Time (min)
240 grit	until planar
320 grit	2
400 grit	2
600 grit	2
800 grit	2
1200 grit	2
6 µm	1
3 µm	1
1 µm	1
Final Polish	0.5

Micrographs were taken at 100x magnification before etching the specimen to assess graphite morphology using ImageJ image analysis software. After establishing a global scale using a watermarked scale bar, a color threshold was placed over the image to include only the nodules. The nodules were then analyzed for count, size, nodularity, and area fraction.

To assess the pearlite and ferrite fractions, the specimens were etched with a 3% nital solution for five seconds, then rinsed and dried. Images were taken at 100x magnification. Using ImageJ, a threshold was used to identify the ferritic areas (white and light gray) to quantify the area fraction of the ferrite. By subtracting the ferrite and graphite fractions from the total area of 1, the area fraction of pearlite was obtained. Any carbides or porosity in the micrographs could have been causes of error in microscopy analyses.

2.5 Porosity Mapping

2.5.1 *Archimedes Density Method*

To determine if any porosity was present, the densities of the sub-riser sections were tested using the Archimedes method. Each specimen was weighed then spray coated with a clear enamel (Rust-Oleum) to avoid rust and graphite water absorption during testing. The mass from the enamel coating (less than 0.003 g) was negligible and the coating's

effective buoyancy force were negligible and therefore did not affect density measurements. A large bowl of distilled water was set on the QCD-1 Specific Gravity and Porosity Measurement System (Q. C. Designs, Inc.). Each specimen was weighed in air, then completely submerged in water on a suspended platform. A detailed procedure is located in Appendix E.

2.5.2 Riser Feed

Each riser was removed from the casting and sliced in half to look at the internal porosity from feeding (Figure 8). To calculate the amount of material fed into the casting, the filled volume of the riser at the pouring temperatures was determined for the 70% compressed sleeve and the 100% compressed sleeve by measuring the volume of water needed to fill the riser sleeve.

Figure 8. Checking test plate 1-15 sub-riser section and removed risers for visual indicators of porosity.

The theoretical density of the liquid ductile iron was calculated based on the amount of carbon and the pour temperature of the iron (Equation 2) [9]. The temperature, T, was measured in degrees Celsius and the carbon was in units of weight percentage.

$$\rho_L = (-9.5 \cdot 10^{-2})\big(wt.\%(C)\big) - (5.5 \cdot 10^{-4})T + 8.042 \qquad \text{Eq. 2}$$

The mass at pouring temperature could then be determined since volume and density were known. Then the difference in the full riser mass and the final riser mass was taken

to determine the mass of material fed into the test plates. This quantifies the shrinking that occurred during solidification.

2.6 Mechanical Testing

2.6.1 Tensile Testing

Tensile bars were machined at Neenah Foundry Co., then tested at Anderson Laboratories, Inc. according to ASTM Standard E8. The gauge length for each tensile bar was 2 inches and the gauge diameter was 0.5 inches. The yield strength, tensile strength, and elongation were measured.

2.6.2 Hardness Testing

Hardness was tested using Brinell Hardness. Each plate was indented five time with a 10 mm indenter tip under a 3000 kgf load and a 15 second indentation time. The indentations were measured with the Brinell Optical Scanning System and Computer Assisted Microhardness System (C.A.M.S). software (NewAge Industries, Inc.).

3 Results

3.1 Casting Outcomes

After breaking out the castings from the sand molds (Figure 9), the removal of the gating system, and sand blasting, the thickness of each plate was measured to assure the quality of the molds. The average thickness of each plate was approximately 1-inch within ± 0.02 inches. The casting surfaces were examined for defects, particularly surface porosity. Test plate 6 had a runout during the casting process and was the only casting with notable surface porosity.

Final casting chemistries were verified by Neenah Foundry using optical emission spectroscopy (OES). The CE values with a target of 4.35 had an average of 4.41±0.1 and those with a target of 4.60 had an average of 4.66±0.03 (Appendix B).

Figure 9. Test Plate 15 directly after breaking out (left) and after removing the riser sleeve (right).

3.2 Microstructure

There is a spread of nodule count and nodule size with ranges of 42 to 190 nodules per square millimeter and averages nodule diameters of 53 to 242 microns (Figure 10 and Figure 11). The nodule count is low compared to an average ductile iron due to a combination of the section thickness and slow cooling rate. The nodule count and nodule size trends are opposite, as expected.

3.2.1 Graphite Nodules

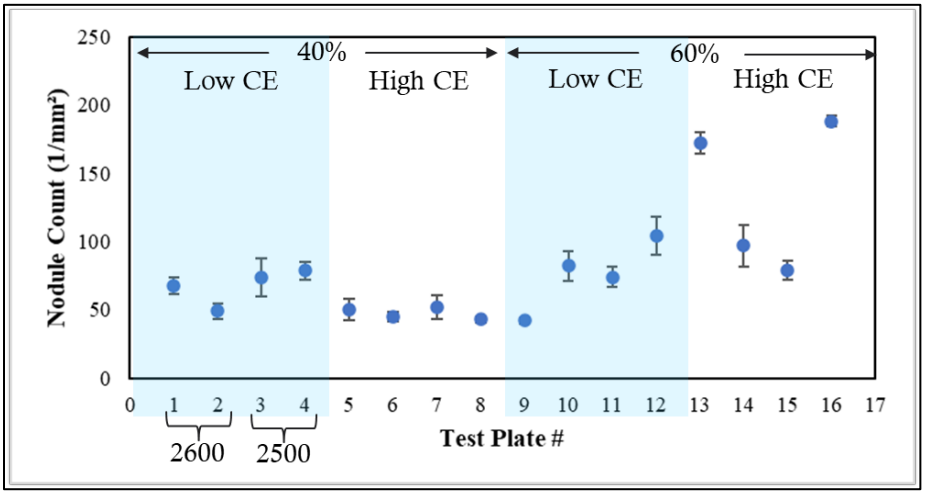

Figure 10. Average graphite nodule count for each test plate with error bars that are the standard error. Runs 9-16 have higher CEs.

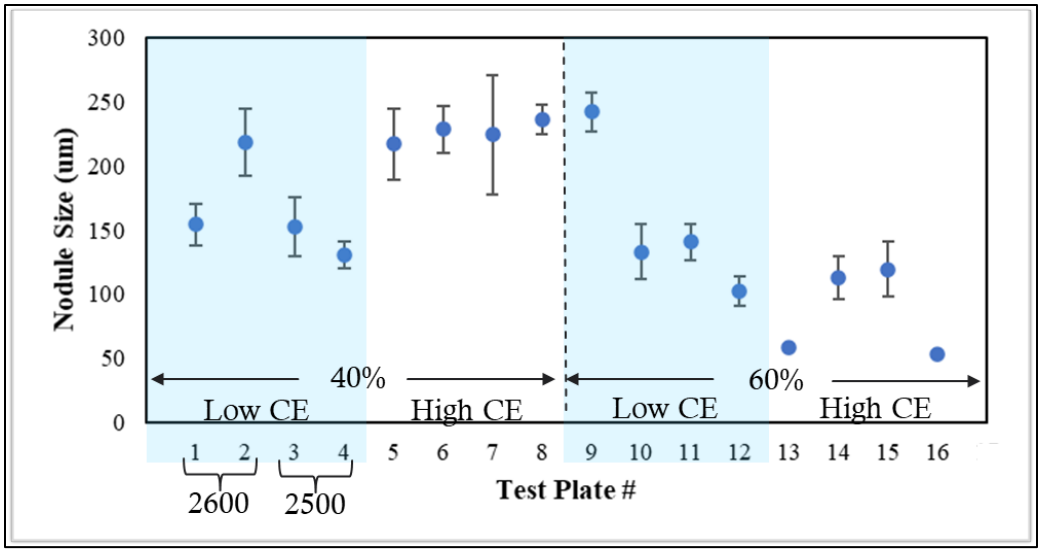

Figure 11. Average graphite nodule size for each test plate. with error bars that are the standard error. CE, return scrap, and temperature levels.

The average nodularity was consistent across all plates at approximately 0.77 to 0.83 nodularity, with two outliers of 0.73 for test plates 5 and 7 (Figure 12). Graphite volume percentage had a range of 6.7 to 17 vol.% and trends upward in test plates that had higher returns (test plates 9-16) (Figure 13). This is a similar trend to the nodule count measurements.

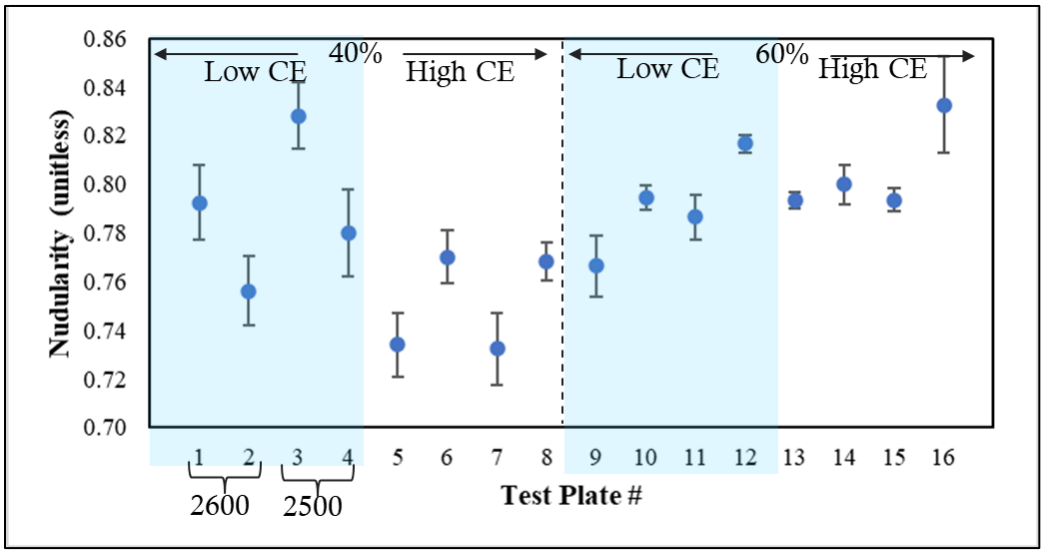

Figure 12. Average graphite nodularity for each test plate with error bars that are the standard error. CE, return scrap, and temperature levels.

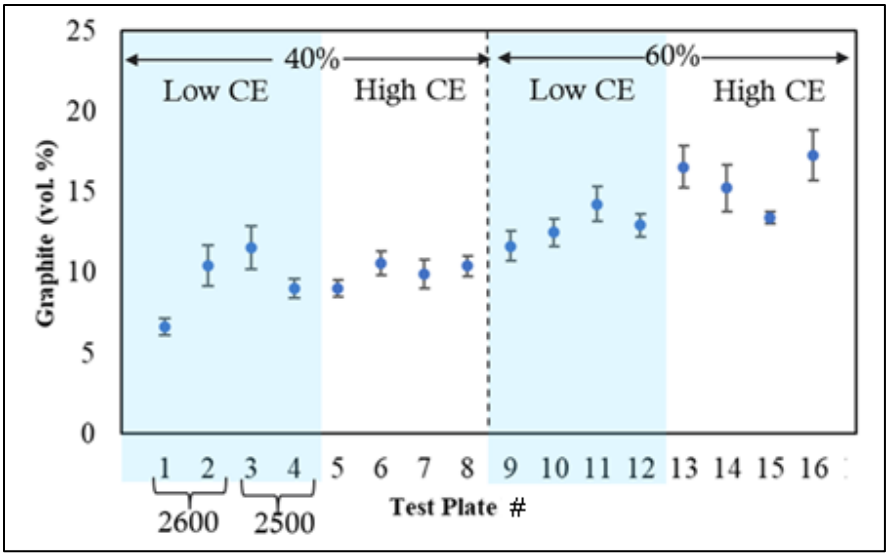

Figure 13. Average graphite content if each test plate measured in volume percent with error bars that are the standard error. CE, return scrap, and temperature levels

3.2.2 Ferrite and Pearlite

The ferrite and pearlite volume fractions vary significantly between each test plate with ranges of 4.50 to 25.7 vol.% and 61 to 89 vol.%, respectively (Figure 14). There is no defined trend observed in the raw data other than that the pearlite and ferrite trends mirror each other. The pearlite errors are propagated since graphite and ferrite were measured and pearlite was calculated as the remaining volume percentage.

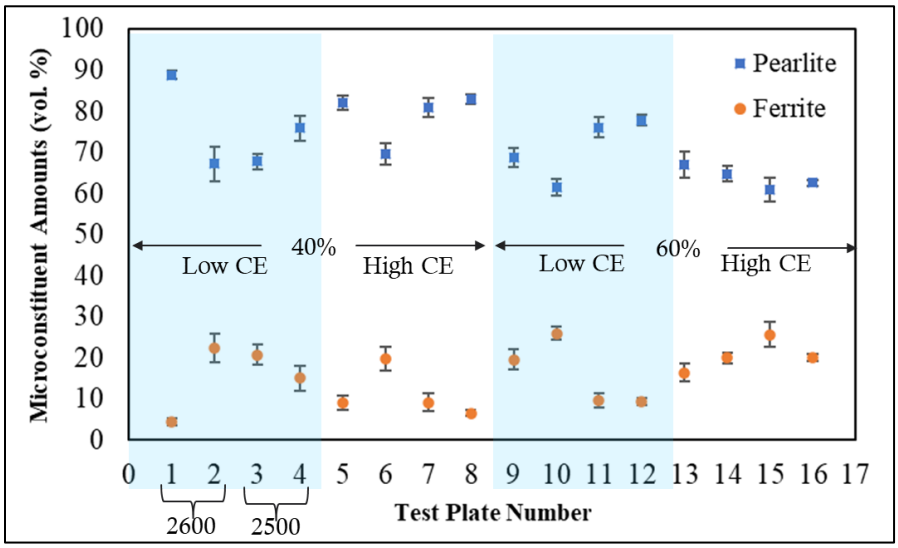

Figure 14. Average pearlite and ferrite volume percentage of each test plate. The error bars the standard error.

3.3 Density

3.31 Sub-Riser Density

Using the Archimedes density method, it was determined that the only casting to contain porosity was test plate 6. As the result of a runout, this casting had an average density of 0.245 lb./in³ (6.76 g/cm³), which was significantly below the accepted density of ductile iron, 0.257 lb./in³ (7.1 g/cm³), and outside of the accepted range for ductile iron density of 0.246 to 0.257 lb./in³ (6.8 to 7.4 g/cm³) [10]. The remaining plates had densities between 0.257 and 0.260 lb./in³ (7.1 and 7.2 g/cm³) (Figure 15).

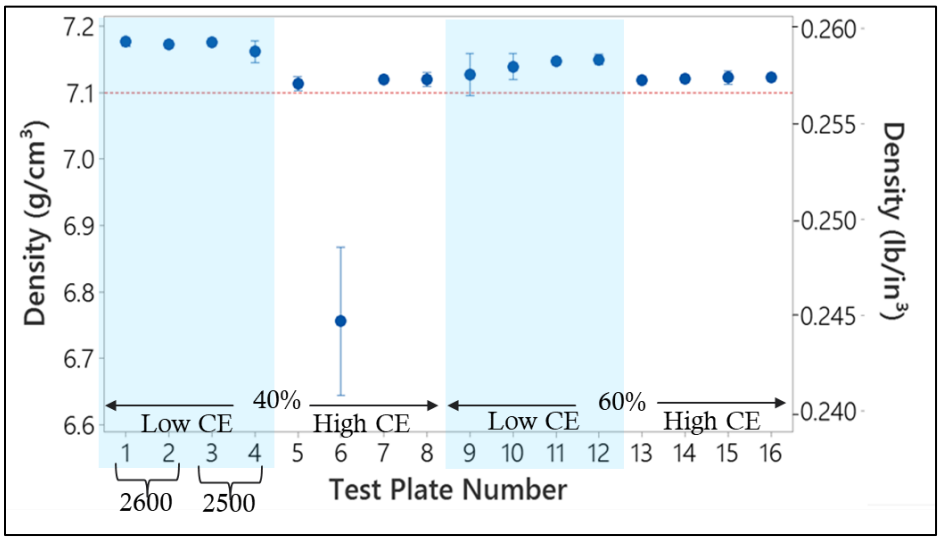

Figure 15. Average Archimedes densities for the sub-riser section of each test plate. The red line indicates the theoretical density of ductile iron (0.257 lb./in³).

3.32 Riser Feed

The sectioned risers all had visible porosity from feeding during solidification similar to the example of test plate 15 in Figure 8. Material fed into the test plates by each riser ranged from 0.23 lbs. to 1.83 lbs. had no immediately clear pattern (Figure 16). Although test plate 6 had porosity from the runout, the material fed was within the range of the other casting at 1.68 lbs.

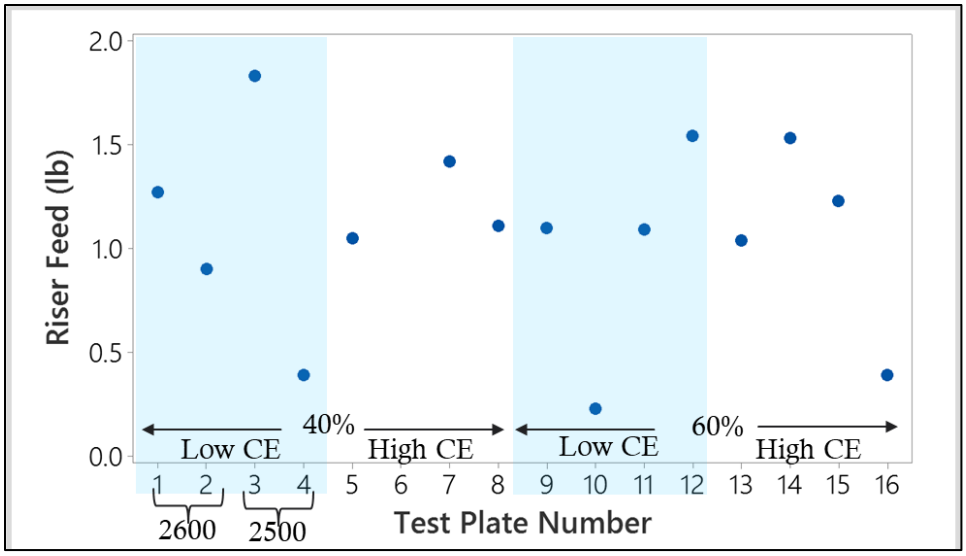

Figure 16. Riser material fed into each casting upon solidification sectioned by CE, return scrap, and temperature levels.

3.4 Mechanical Properties

3.4.1 Strength and Elongation

Tensile testing provided information on the yield strength, tensile strength, and elongation of each set of casting conditions. Due to uncontrollable circumstances, rather than four tensile bars per casting, there were between two and four tested as indicated in Table 4. Any plates with only one data point listed had a defect in the tensile bar, causing premature failure. These were not included in statistical analyses.

Table 5. Strength and elongation results for each test plate. The number of data points is specified since they are not consistent.

Test Plate Number	Avg. Tensile Strength (ksi)	Avg. Yield Strength (ksi)	Avg. Elongation (%)	# of Data Points
1	111	59	5.8	2
2	113	60	5.5	2
3	112	60	5.8	2
4	106	65	5.1	4
5	112	65	6.8	2
6	107	65	4.5	2
7	108	65	5.0	2
8	111	62	7.0	1
9	112	62	5.5	2
10	108	61	5.0	4
11	103	61	5.0	2
12	114	62	7.0	1
13	104	64	5.0	4
14	112	65	7.3	2
15	106	65	5.0	2
16	110	66	4.6	4

Although the data points were not consistent, the resulting average tensile strength, yield strength, and elongation were plotted in Figure 17 and Figure 18. Tensile strength has no obvious trends; however, mold hardness may carry influence. Yield strength is mostly consistent for high CE values versus low CE values and the castings with greater strengths correlate to high CE values. Contrarily, elongation had no obvious trends.

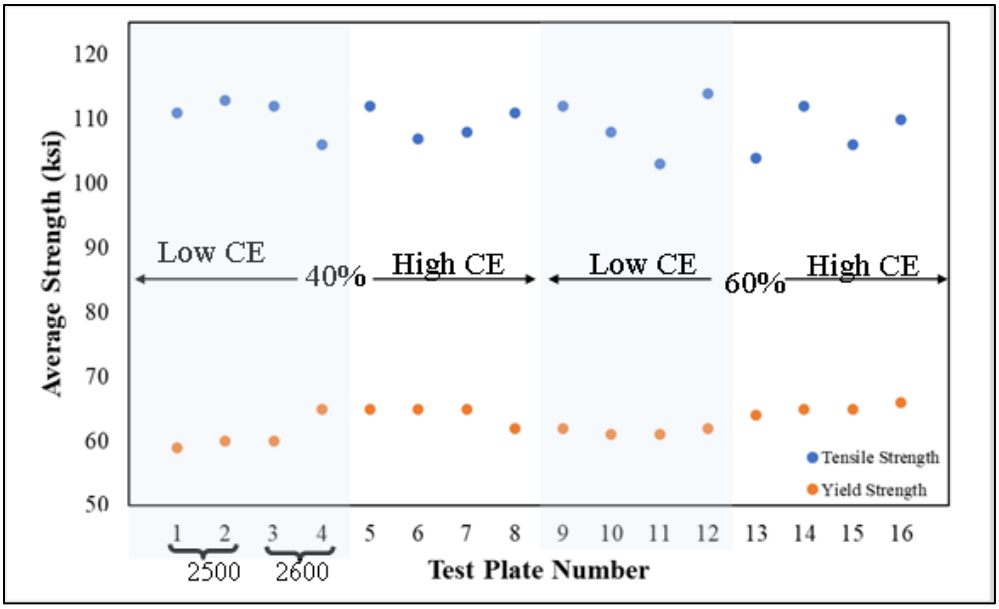

Figure 17. Average tensile and yield strengths for each test plate sectioned by CE, return scrap, and temperature levels.

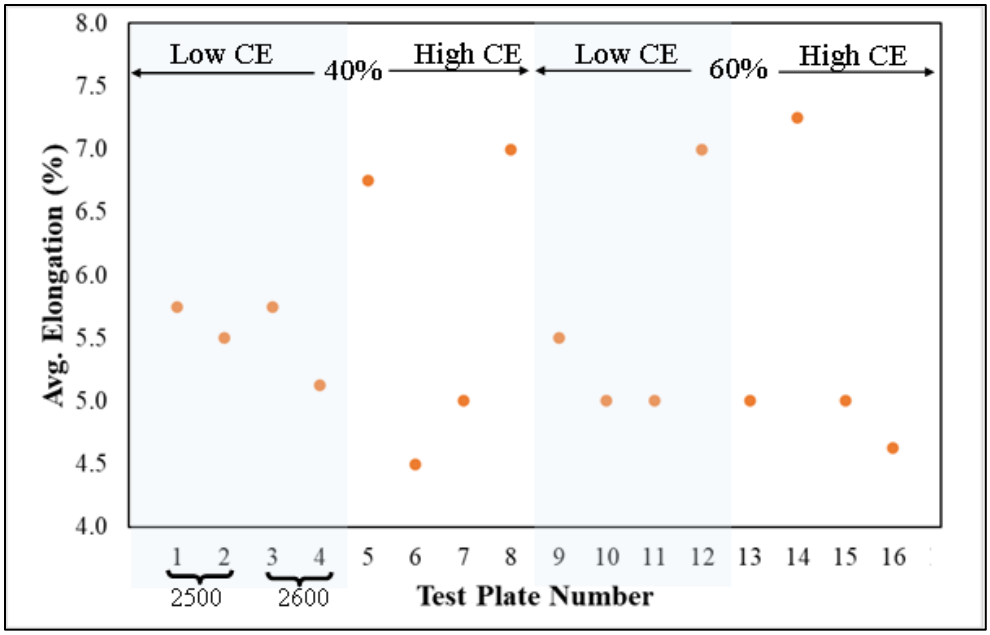

Figure 18. Elongation during tensile testing of each test plate sectioned by CE, return scrap, and temperature levels.

3.4.2 Hardness

Brinell hardness values for the individual test plates were consistent. The plates that had 60% return scrap (test plates 9-16) had slightly greater hardness values in the range of

252 to 265 BHN as compared to 236 to 254 BHN for the castings with 40% return scrap (Figure 19). Test plate 1 had a significantly lower hardness value than all other castings.

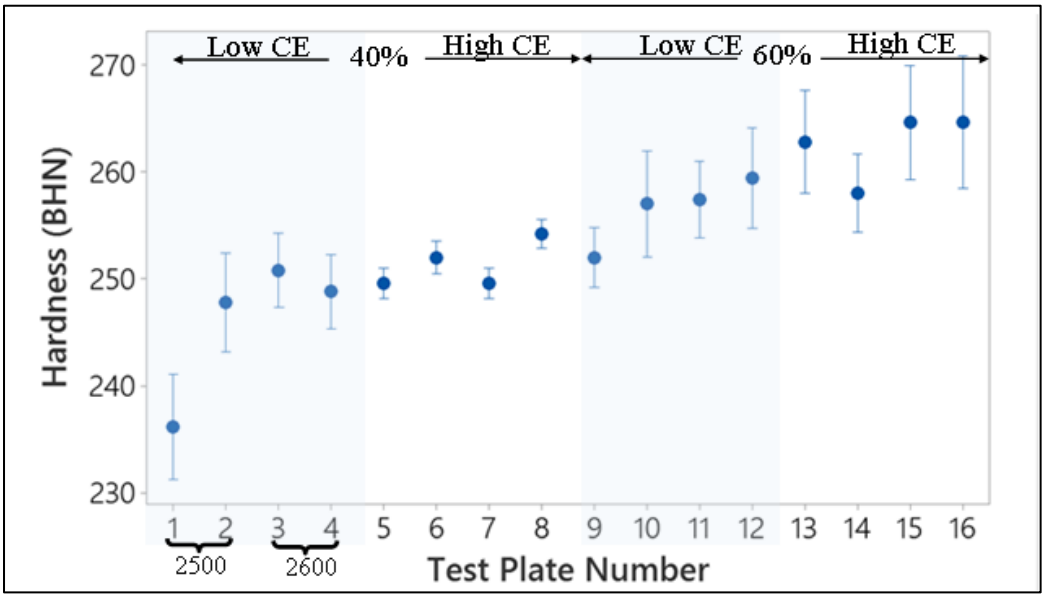

Figure 19. Brinell hardness values taken with a 10mm indenter and 3000 kgf load. The error bars are 95% CI of the mean.

4 Discussion

4.1 Microstructure

The results from the microstructural analyses were analyzed in Minitab 2019 software (Minitab LLC.) as a general linear model to understand factor-response relationships, if any were present. The significance levels were set at 95% confidence levels, therefore any p-value less than or equal to 0.05 indicated a significant effect. Mold hardness was determined to be statistically insignificant for all responses except riser feed and elongation, and therefore was removed from all models unless specified.

4.1.1 Graphite

Graphite nodule count and size are known to be related to tap temperature, cooling rate, and composition [7]. There is clearly an effect on nodule count as a response to CE ($p=0.03$) and return scrap ($p=0.00$) (Figure 20) and an effect on nodule size as a response to return scrap and pour temperature. As expected, the nodule count is greater for higher CE because carbon and silicon are graphitizers. Additionally, an increase in return scrap

provides more nucleation sites for graphite nodules, promoting heterogeneous nucleation, allowing growth to occur sooner than if nucleation sites were not present [6]. It follows that the nodule size is larger for the castings poured at lower CE and return scrap percentages because there were less nucleation sites and a lower driving force for graphite nucleation, requiring more time and energy to nucleate before growth occurred.

An increased pour temperature tends to increase nodule size significantly, with a p-value of 0.03. The extra 100°F superheat in this case did not burn off more carbon than the lower pour temperature or increase the effectiveness of the magnesium treatment due to the experimental set up. Instead, the casting at higher temperatures had less carbon burn off and magnesium treatment fade because the castings were poured first chronologically. The higher temperature at pouring caused the casting to effectively cool slower, resulting in the smaller nodules diffusing into the larger nodules. This should have also statistically affected the nodule count by decreasing it further since the nodules would have been much larger with more time for growth before solidification.

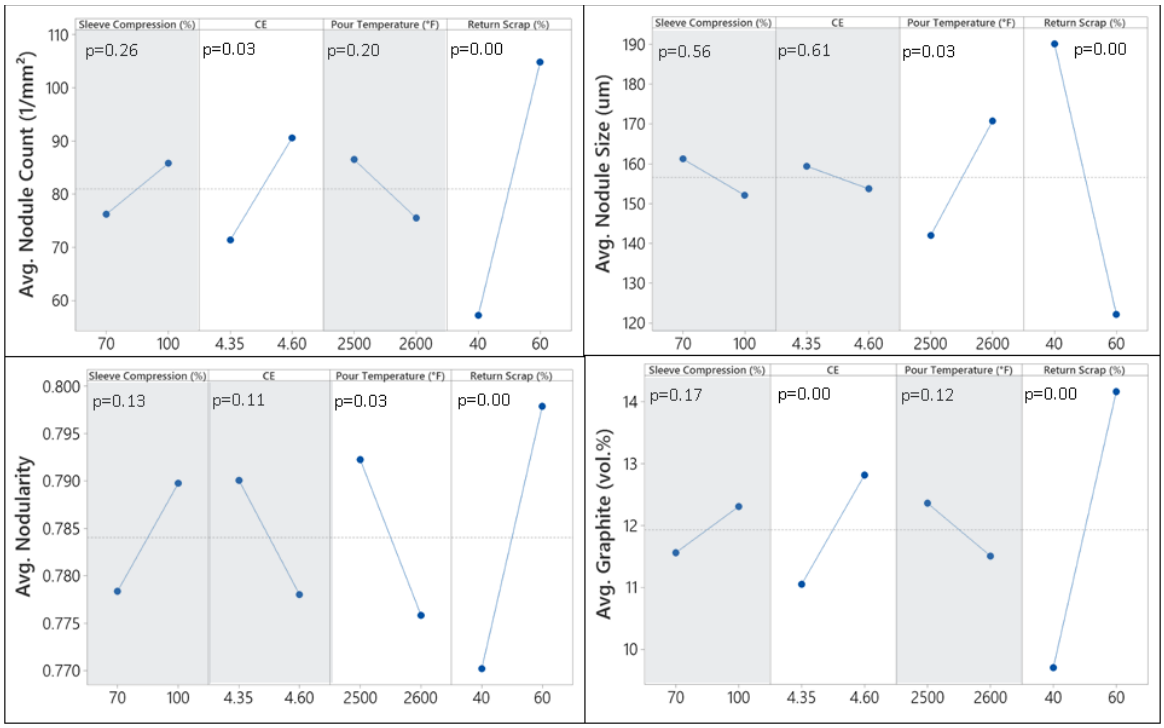

Figure 20. Main effects plots for graphite nodule count, graphite nodule size, nodularity, and graphite volume percentage in relation to each casting condition. Grey sections had statistically insignificant main effects.

Nodularity, or circularity, was influenced primarily by pour temperature and return scrap percentage. Magnesium is highly correlated to nodularity and having insufficient magnesium will significantly impact the graphite morphology. A higher pouring temperature increases magnesium fade, therefore, in theory, the castings poured at 2600°F would have had significantly lower nodularity than those poured at 2500°F [7]. However, since both pouring temperatures came from the same heat, and magnesium fade would have occurred between pouring the 2600°F and 2500°F castings, the nodularity should be less for the lower pouring temperature. This was not the case, however test plates 13-16 had a magnesium content 0.04 above the target, which could have contributed to the formation of some exploded graphite in the higher temperature castings before magnesium fade occurred for the lower temperature castings.

Although CE was not statistically significant for nodularity, if CE is raised too high, there could be issues with exploded graphite [6]. Although this situation was not present for this set of experimental results, it should be noted that this could impact nodularity.

There may be error in nodule size and nodularity due to graphite pull-out during polishing. Too much pressure, particularly when grinding with coarser grits can cause the graphite nodules to detach and fall out of the sample. This can cause an over-estimate of nodule size and may account for the low nodularity measurement.

Graphite volume percentage reflects the main effects trends of graphite nodule count for each factor. This result is congruent with expectations since the amount of carbon out of solution increases with CE and return scrap percentage. The sleeve compression and pour temperature did not have statistically significant effects on amount of graphite, however, the general linear model showed that there was an interaction between CE and pour temperature that suggests a variation of nearly 3 vol.% graphite between a CE of 4.35 and 4.60 at 2600°F. This is likely due to the carbon burn off and magnesium fade that occurred in the time between casting the 2500 and 2600°F decreasing nodule nucleation and thereby graphite percentage for the lower temperature castings.

Additionally, in the castings with more return scrap, the relative percentage of steel scrap was decreased. The resulting lower sulfur content may have increased the magnesium recovery rate.

4.1.2 Ferrite and Pearlite

Ferrite and pearlite volume percentages give an indication of the strength of the alloy. A 100-70-03 ductile iron is expected to have 80 vol.% or more of pearlite [7]. Since there was a range of 61-89 wt.% pearlite, it is not expected that all the castings will meet the 100-70-03 grade. The statistically significant factors for both ferrite and pearlite formation was return scrap percentage (Figure 21). An increase in return scrap correlates with nearly a 10 wt.% decrease in pearlite. This is the result of increased graphite nodule formation because the graphite has more nucleation sites, which pulls more of the carbon to nodules before it can form the lamellar pearlite structure. The trends in ferrite and pearlite percentages clearly oppose each other, as expected, since pearlite is comprised of 87.5 wt.% ferrite (and 12.5 wt.% Fe_3C) [2].

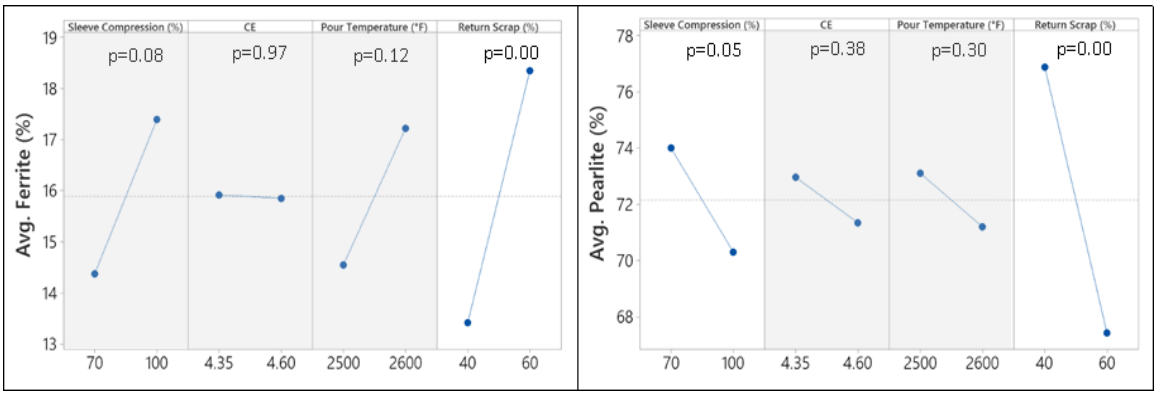

Figure 21. Main effects plots for ferrite and pearlite volume percentages

A greater percentage of pearlite was formed with a sleeve compression of 70% likely due to the increased neck length of the riser which froze off more quickly than the 100% compression. With the 100% compressed sleeve, the hot riser was closer to the casting which promotes ferrite formation. An increased solidification rate is attributed to increased pearlite formation which reduces the diffusion of carbon from solution to contribute to nodule growth, leaving behind ferrite.

4.2 Density

4.2.1 Sub-Riser Density

Test plate 6 had a runout during pouring, potentially altering results, therefore the results from test plate 6 were removed as outliers. The average density of each test plate was compared to the theoretical density of 7.1 g/cm³ by a calculated percent error (Table 6). The largest error was 1.1 wt.%, excluding test plate 6, therefore it was determined that none of the castings had internal porosity.

Table 6. Average Archimedes densities for each test plate and the percent error from the theoretical density of 7.1 g/cm³

Plate Number	Avg. Density (g/cm³)	Stand. Dev.	Error (%)
1	7.18	0.004	-1.1
2	7.17	0.003	-1.0
3	7.18	0.003	-1.1
4	7.16	0.01	-0.9
5	7.11	0.007	-0.2
6	6.76	0.07	4.8
7	7.12	0.003	-0.3
8	7.12	0.007	-0.3
9	7.13	0.02	-0.4
10	7.14	0.01	-0.5
11	7.15	0.003	-0.7
12	7.15	0.005	-0.7
13	7.12	0.001	-0.3
14	7.12	0.001	-0.3
15	7.12	0.006	-0.3
16	7.12	0.001	-0.3

Density of the sub-riser sections of the test plates was primarily correlated to the CE and return scrap (Figure 22).

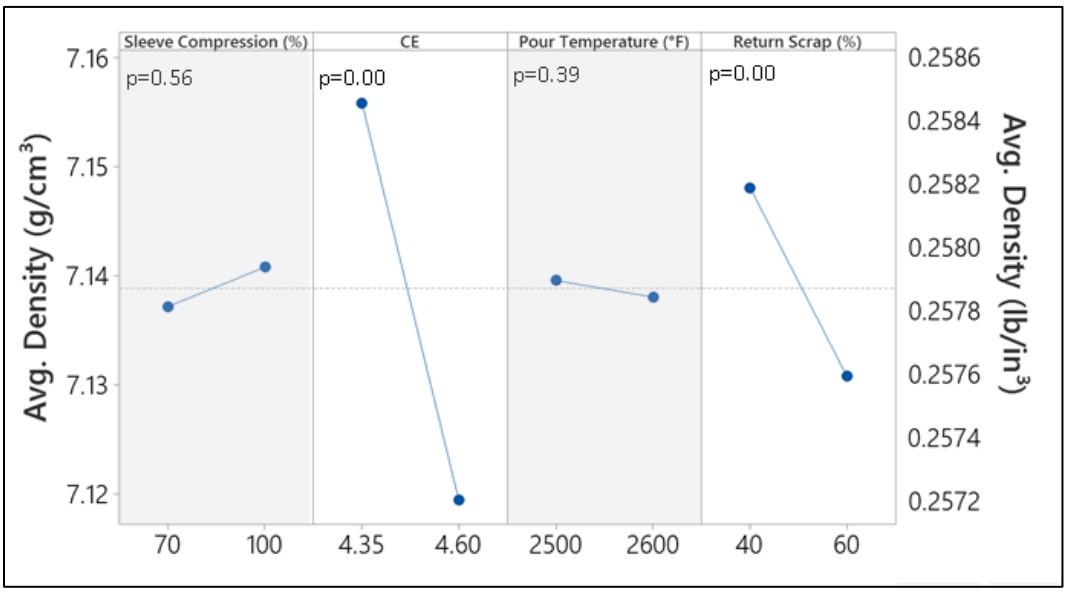

Figure 22. Main effects plot for the sub-riser density of the test plates

It was discussed previously that the graphite nodule count and volume percent increased with higher CE and return scrap. This in converse to the effects of CE and return scrap on density, indicating a relationship between the graphite amount and density. A regression analysis was performed which determined a predictive equation with an R^2 value of 0.723 (Equation 3). Return scrap (RS) is in units of percentage and the density is in units of lb/in^3.

$$\rho = -0.005CE - 0.00003RS + 0.282 \quad \text{Eq. 3}$$

Graphite has a density of 0.081 lb/in^3 (2.23 g/cm^3) [5] whilst ferrite has a density of 0.282 lb/in^3 (7.81 g/cm^3) [3], and pearlite has a density of 0.277 lb/in^3 (7.67 g/cm^3) [4]. A purely ferritic matrix with an average of 12 vol.% graphite nodules would have a theoretical density of 0.258 lb/in^3 (7.14 g/cm^3). This is substantially less dense compared to the theoretical density of a completely pearlitic alloy. As a result, the increase in graphite at higher CE return scrap levels corresponds to a decrease in density because there are more nodules since carbon in the form of graphite nodules is significantly less dense than the carbon in the Fe_3C of pearlite. The decrease in density is small at about a 0.5% difference, however it is noticeable and potentially significant for mechanical properties.

4.2.2 Riser Feed

The riser feed was only correlated to sleeve compression and mold hardness (Figure 23). CE was removed from the model during the process of model simplification due to the lack of correlation. Although CE did not show a significant effect on riser feed in these castings, other studies have determined that higher CE can decrease shrinkage [7].

The pouring temperature did not have a significant effect on the riser feed. It would follow that a higher pouring temperature would increase the feeding time and therefore increase the material fed, however this was not the case. In a well-designed riser system, there is the ability for the riser to feed well within a range of temperatures, which may attribute to the lack of effect of the pouring temperature on riser feed.

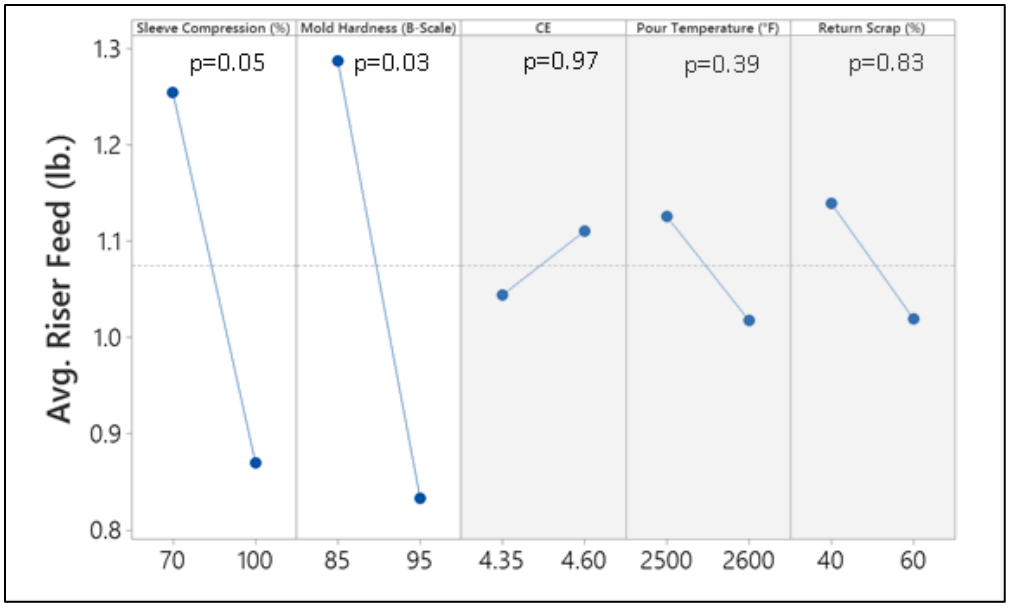

Figure 23. Main effects plot for the mass of iron fed by the riser

A sleeve compression of 70% correlated to more material fed into the casting. Although the neck was longer on these risers, the added volume of material contributed more material to the casting. Additionally, the extra volume in the riser increased the thermal mass of the riser, potentially negating the effects of the neck length. It is possible that the sprue did feed the casting slightly, however the solidified sprue height was not significantly lower than that of the mold upon visual inspection.

A lower mold hardness of 85 is more likely to deform during casting than a mold with 95 hardness (B-scale) in terms of swelling or mold wall movement.

During solidification, graphite expansion can deform the mold, effectively adding more volume to the mold, requiring more metal to properly fill the casting. This contributes to increased shrink [7]. A higher mold hardness reduced the shrink in the casting because it is less likely to deform and thereby decreases the amount of material needed to be fed into the casting upon solidification.

4.3 Mechanical Properties

4.3.1 Strength and Elongation

All the castings failed to meet the 70 ksi yield strength, however most achieved the tensile target of 100 ksi and all hit the elongation target of 3%. An increase in yield strength was significantly correlated with increased CE and return scrap (Figure 24). Yield strength should be increased with a higher pearlite content; however, this was not the case as the yield strength CE and return scrap main effects opposed those of pearlite. They do follow the trends for graphite volume percentage. Increased graphite nodules typically decrease strength because graphite is soft and does not act as a dislocation barrier. In this case, the increased graphite kept the excess copper in solution, contributing to solid-solution strengthening. This, however, does not explain the entire 5 ksi increase in yield strength from CE nor the increase form return scrap.

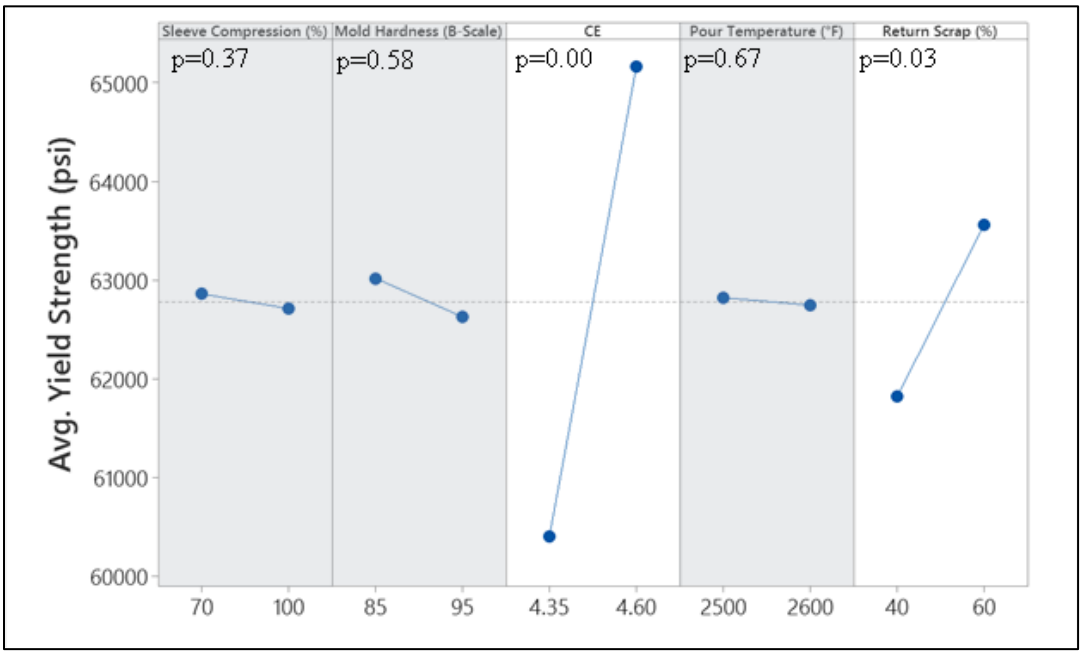

Figure 24. Main effects plot for the average yield strength of each test plate. Insignificant factors are grey.

Tensile strength did not have any significant correlations to the casting factors (Figure 25). Tensile strength influenced by a multitude of factors including pearlite volume fraction and graphite morphology.

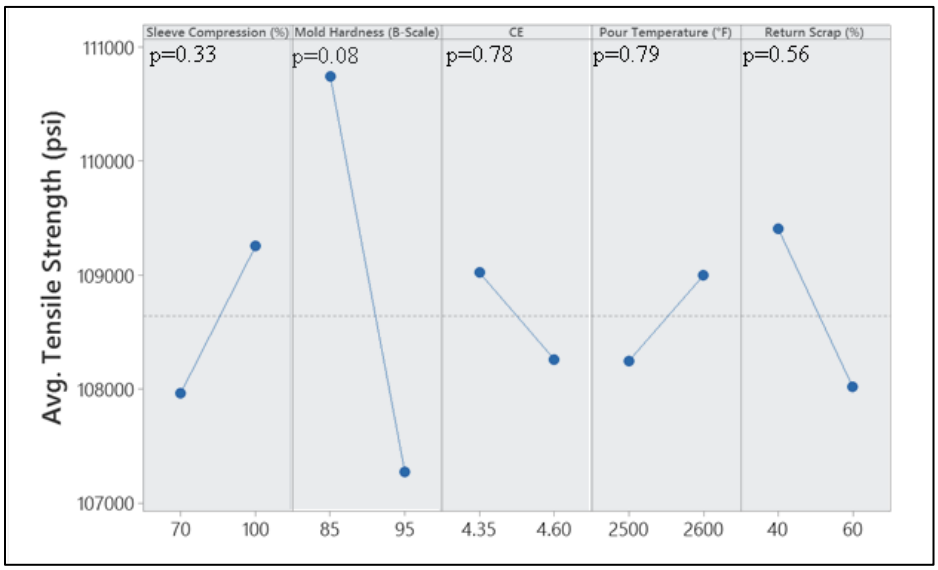

Figure 25. Main effects plot for the average tensile strength of each test plate. Insignificant factors are grey.

Elongation is a critical property of ductile iron because it reduces the chance of a brittle fracture that could be catastrophic in a critical component. Elongation was negatively correlated to an increase in mold hardness with a p-value of 0.04. No explanation was determined for this behavior.

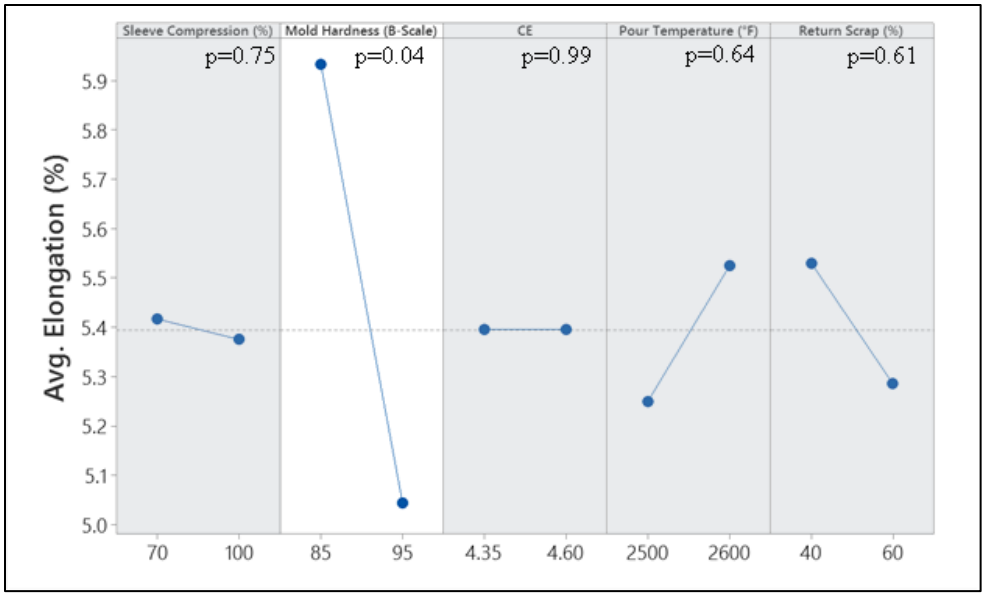

Figure 26. Main effects plot for elongation during tensile testing of each test plate. Insignificant factors are in grey.

Tensile strength, yield strength, and elongation are all connected which confounds the results. Tensile strength and elongation are inversely related, however that is only seen in the sleeve compression trend and CE [10].

Caution should be taken with the tensile data results and statistics since the sample size was small for most castings. Further tensile testing must be done before any regression analysis can be accurately performed.

4.3.2 Hardness

Brinell hardness was influenced by all factors except mold hardness (Figure 27). Despite the runout of test plate 6, the Brinell hardness was in the same range as the remaining plates, therefore it was included in this analysis. No porosity was visible in the hardness specimen.

The CE and return scrap percentage trends are opposite of those seen for pearlite, which is counterintuitive since pearlite fraction contributes to an increase in hardness [11]. However, the CE was primarily increased with silicon for this research and silicon is known to increase hardness in ductile irons that do not have fully-ferritic matrices [12].

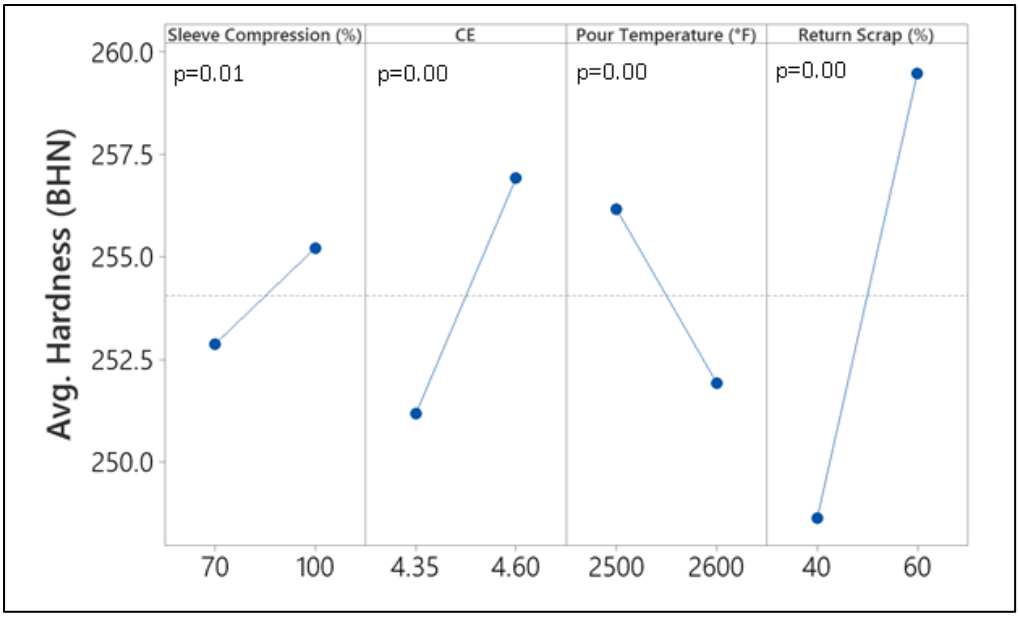

Figure 27. Main effects plot for Brinell hardness of the test plates

A regression analysis was performed to quantify the relationships between Brinell hardness and the casting factors (Equation 4). Sleeve compression (SC) is in units of percentage, the pour temperature (T_p) is in degrees Fahrenheit, and return scrap (RS) is measured in percentage (Equation 4). The R^2 value was 0.746.

$$HBN = 0.078SC + 23CE - 0.043T_p + 0.543RS + 225.7 \quad \text{Eq.4}$$

The sleeve compression contributed the least to the Brinell hardness calculation, followed by pour temperature. The most influential factor was return scrap.

5 Future Work

The ICME approach relies on a large and broad database to make useful and accurate predictions. To further comprehend the100-70-03 ductile iron casting system, research will continue with an emphasis on the molding parameters and section thickness. The sand type, such as chemically bonded compared to green sand, or a combination of both will be examined along with factors of green sand mold hardness and casting section thickness. The pouring temperature and CE of the ductile iron will also be considered as factors with responses of cooling rate, microstructural attributes, shrink porosity, strength and elongation, and hardness. Quantification of these results, along with those of the

current study, using empirical and mechanistic correlations, will be a critical step in creation and validation of the ICME database and predictive capabilities.

6 Conclusion

Standard foundry variables of CE, return ratio, mold preparation, riser feed, and casting temperature play significant roles in forming the microstructure and mechanical properties of ductile iron. Although the 100-70-03 grade has specifications, the process and microstructure can vary significantly to achieve the same result. Although the target grade of 100-70-03 was not achieved in this study, relationships were seen and determined between casting process, the microstructure, and the basic mechanical properties.

Return scrap was significantly correlated to all experimental factors, except for riser feed, tensile strength, and elongation. More return scrap provides additional graphite nodule nucleation sites and increased the nodule count and graphite volume percentage in the microstructure. This resulted in an influence on density, hardness, strength, and elongation. Density decreased by approximately 0.05% when the fraction of graphite nodules was greater due to the low density of graphite. A greater percentage of return scrap and higher CE level correlated to increased graphite nodule formation and count which resulted in increased density and hardness. In this study, pearlite and hardness do not correlate, which is opposite from known ductile iron behavior.

Sleeve compression significantly contributed to the amount of material fed into a casting and is an inexpensive change that can be instantly implemented into a foundry that already employs this technology. In addition, a mold hardness of 95 (B-scale) appeared to be more effective than a mold hardness of 85 (B-scale) at reducing shrink; thereby reducing the material needed to be fed into the casting to counter shrink. Additionally, mold hardness had an influence on elongation. However, mold hardness in the range of 85 to 95 B-scale was not statistically correlated to any other casting factors.

Future work will be instrumental in expanding the ICME database to encompass the 100-70-03 pearlitic ductile iron system to facilitate accurate virtual predictions to aid in creation and validation of an industrial ductile iron ICME predictive program.

7 References

[1] P. Stanislaw and R. Zuczek, "The Use of ICME Process to Design a Rocker Arm for Special-Purpose Vehicles," *Commission of Motorization and Energetics in Agriculture,* vol. 12, no. 1, pp. 205-210, 2012.

[2] M. A. Yescas-Gonzalez and H. K. D. H. Bhadeshia, "Cast Irons," University of Cambridge, [Online]. Available: https://www.phase-trans.msm.cam.ac.uk/2001/adi/cast.iron.html. [Accessed March 2020].

[3] M. D. Chermahini, S. Sharafi, H. Shokrollahi and M. Zandrahimi, "Microstructural and Magnetic Properties of Nanostructured Fe and Fe50Co50 Powders Prepared by Mechanical Alloying," *J. Alloys Compd. ,* vol. 474, pp. 18-22, 2009.

[4] E. P. Elsukov, V. M. Fomin, D. A. Vytovtov, G. Dorofeev, A. V. Zagainov, N. B. Arsent'eva and S. F. Lomaeva, "Structural and Phase Transformations During Isothermal Annealing of Mechanically Alloyed Iron-Amorphous Fe-C Phase Nanocomposite: Formation of Cementite," *Phys. Met. Metallogr.,* vol. 100, pp. 251-269, 2005.

[5] A. E. Juarez, F. A. Schroder, B. M. Avalos, B. Winkler, L. Bayarjargal, A. Friedrich, Y. V. Milman, D. R. Kammler, S. M. Clark, J. Yan and M. Koch Muller, "Formation of Scandium Carbides and Scandium Oxycarbide from the Elements at High-(p,T) Conditions," *J. Solid Scate Chemistry,* vol. 183, pp. 975-983, 2010.

[6] Ductile Iron Society, "Effect of Carbon in Ductile Iron," *Hot Topics,* no. 6, 2003.

[7] D. I. Society, "Ductile Iron Quality Assurance Guide," Ductile Iron Society, 2018.

[8] Foseco International Linited, "Vesuvius Feeding Systems for Iron Castings," 2020. [Online]. Available: https://www.vesuvius.com/en/our-solutions/international/foundry/iron-foundry/feeding-systems.html#titleLink-4. [Accessed November 2019].

[9] M. Wrobel, A. Burbelko and D. Gurgul, "Modelling of Change in Density of Nodular Cast Iron During Solidification Using Cellular Automation," *Archives of Metallurgy and Materials,* vol. 60, no. 4, 2015.

[10] Ductile Iron Society, "Ductile Iron Data for Design Engineers," Ductile Iron Society, [Online]. Available: https://www.ductile.org/didata/Section3/3part2.htm#Density. [Accessed 12 May 2020].

[11] R. A. Gonzaga, P. Martinez Landa, A. Perez and P. Villanueva, "Mechanical Properties Dependency of the Pearlite Content of Ductile Iron," *Journal of Achievements in Materials and Manufacturing Engineering,* vol. 33, no. 2, pp. 150-158, 2009.

[12] Ductile Iron Society, "Silicon and its Effects in Ductile Iron," *Hot Topics,* vol. 2000, no. 10, p. 10, 2000.

[13] M. A. Yescas-Gonzalez, "Dissemination of IT for the Promotion of Materials Science (DoITPoMS)," Department of Materials Science and Metallurgy, University of Cambridge, 3 July 2018. [Online]. Available: https://www.doitpoms.ac.uk/miclib/micrograph_record.php?id=782. [Accessed March 2020].

8 Appendices

8.1 Appendix A: Test Plate and Riser Images

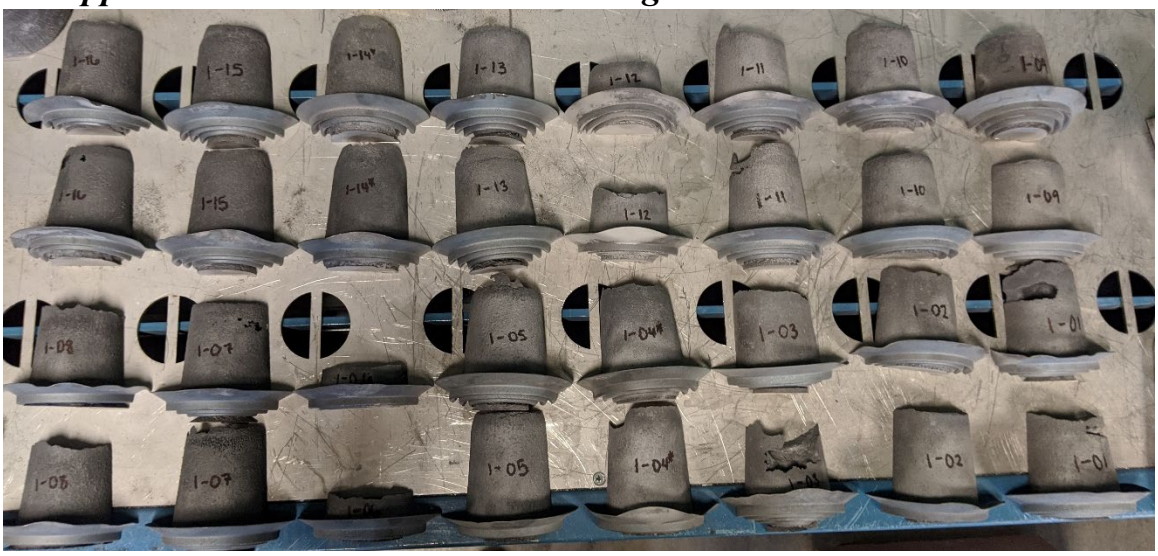

Figure A1. Visual comparison of the heights of the solidified risers with metal breaker cores from the riser sleeve still attached.

Figure A2. Visual assessment of riser feed with metal breaker cores from the riser sleeve still attached.

8.2 Appendix B: Actual Casting Conditions and Microstructural Results

Table B1. Actual experimental casting conditions from the test plate casting process

Run Number	Sleeve Compression (%)	Mold Hardness (B-Scale)	CE	Pour Temperature (°F)	Charge Returns (%)	our Time (s)	late Thickness (in.)
1	70	94	4.32	2630	39.4	19	.01
2	100	86	4.32	2590	39.4	20	.03
3	70	87	4.32	2490	39.4	15	.01
4	100	95	4.37	2390	38.2	13	.01
5	70	89	4.68	2660	38.7	16	.03
6	100	95	4.68	2620	38.7	17	993
7	70	97	4.68	2510	38.7	19	.03
8	100	84	4.68	2460	38.7	13	.02
9	70	86	4.48	2660	56.0	16	979
10	100	95	4.48	2630	56.0	24	988
11	70	95	4.48	2520	56.0	18	.03
12	100	87	4.48	2470	56.0	13	943
13	70	95	4.63	2620	58.2	17	985
14	100	87	4.64	2540	58.2	14	988
15	70	85	4.63	2450	58.2	14	.00
16	100	95	4.63	2420	58.2	14	950

Table B 2. Average microstructural features of each ductile iron test plate

Test Plate Number	Avg. Nodule Count (nod/mm²)	Avg. Nodule Size (um)	Avg. Nodularity (%)	Avg. Ferrite (%)	Avg. Pearlite (%)	Avg. Graphite (%)
1	67	154	79	4.5	89	6.7
2	49	219	76	22	67	10
3	61	153	83	21	68	12
4	79	131	78	15	76	9.0
5	50	217	73	9.0	82	9.0
6	45	229	77	20	70	11
7	52	225	73	9.2	81	9.9
8	43	237	77	6.6	83	10
9	42	242	77	20	69	12
10	82	133	79	26	62	13
11	74	141	79	9.7	76	14
12	100	102	82	9.3	78	13
13	170	58.5	79	16	67	17
14	97	113	80	20	65	15
15	79	120	79	26	61	13
16	190	53.2	83	20	63	17

8.3 Appendix C: Tinker Omega TOM-125 Chemically Bonded Sand Molding SOP

- Check the sand level by assuring that the super sack above the sand tank does not need to be replaced (Figure C1).

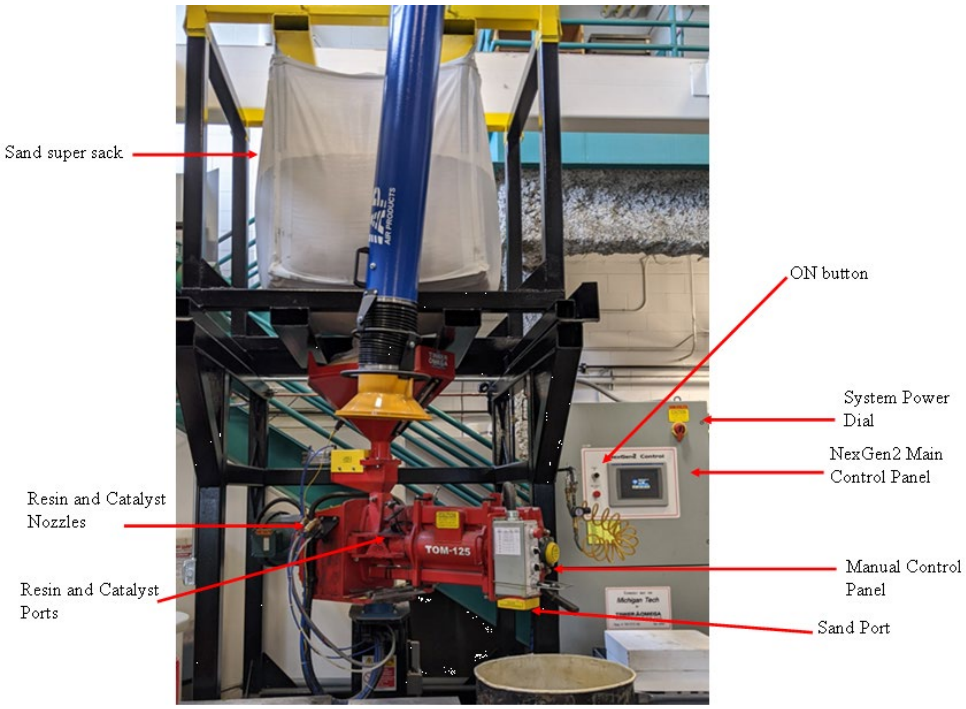

Figure C1. Tinker Omega TOM-125 Chemically Bonded Sand Molding setup

- Check the resin and catalyst nozzles as well as each port to ensure they are clean and not blocked.
- The sand dispensing port should be cleared of sand. If it is not, use a ribbed aluminum rod to clear it out whilst the emergency stop is pushed. Do NOT put your hands in the chute.
- Turn the dial on the upper right-hand side of the NexGen2 control panel clockwise to the ON position. Press the Green START button until it is illuminated (Figure C2).

Figure C2. NexGen2 main control panel for the Tinker Omega TOM-125

- On the main screen of the control panel, select the button labeled “Run Screen”, then select “Manual Screen”. The resulting display is shown in Figure C3.

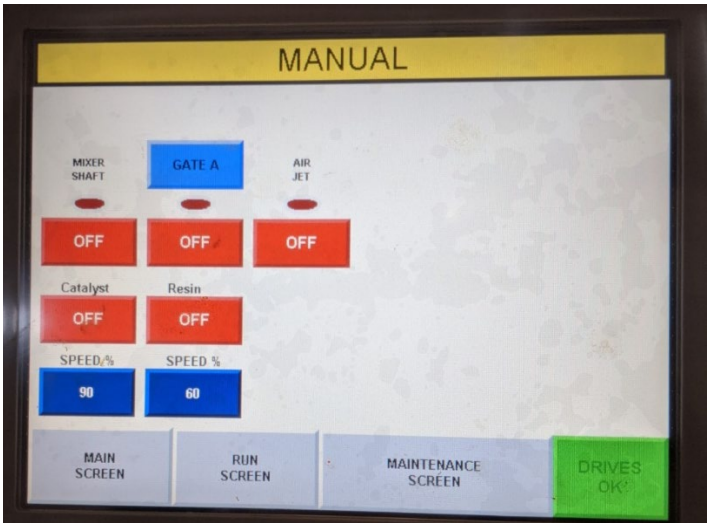

Figure C3. Manual screen of the NexGen2 control panel

- Take a recycled container from the shelf next to the instrument and hold the nozzles over it. Press the red “Resin” button and let the resin flow for 3-5 seconds. Select the same button again to shut it off. Repeat for the catalyst to ensure proper flow.
- Insert the resin nozzle into the left port and the catalyst nozzle into the right port. Align the brace and tighten it just enough to hold the nozzles in place (Figure C4). Do not overtighten.

Figure C4. Resin and catalyst nozzles situated in their respective ports

- On the main control panel, select “Run Screen” then select the green AUTO MODE button resulting in the display shown in Figure C5.

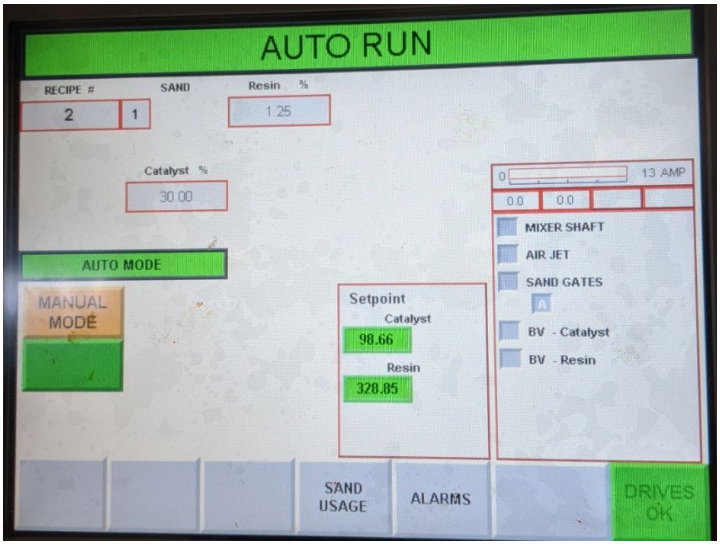

Figure C5. Auto run screen of the NexGen2 control panel

- On the user control panel, rotate the knobs to “A” and “2” (Figure C6).

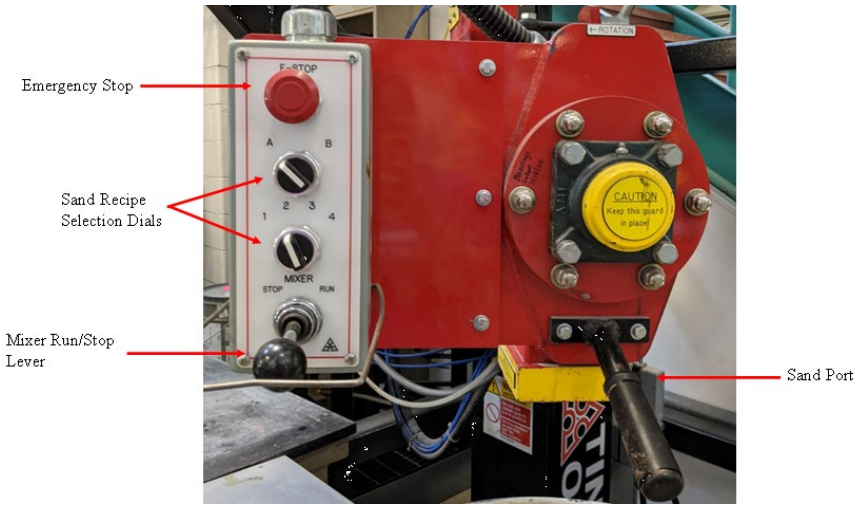

Figure C6. User control panel

- Place the sand chute over the waste bucket and tap the lever to the RUN position then release it. Allow the sand to run out for 5-10 seconds to avoid any unmixed sand. Nudge the lever to the left to the STOP position. The sand and air will continue to run out for a few more seconds.
- Put on a pair of nitrile gloves.
- Set the flask with the pattern on the table next to the instrument (drag side up). Lightly dust the pattern with parting compound.
- With the chute over the waste bucket, switch the lever to the RUN position and let it run for 3 seconds before quickly positioning the chute over the flask.
- Pack the sand down gently by hands as the flask fills. Let the flask overfill slightly, then move the chute back over the waste bucket and tap the lever to the STOP position.
- Using the aluminum bar, pack down the sand on the top of the pattern and strike off the excess sand.
- Allow the pattern to cure for 10-15 minutes, then remove the pattern.
- Remove the nozzles from their ports. Soak the resin nozzle in water and the catalyst nozzle in kerosene (found in the flammables cabinet). Ensure that they

are cleared out then place them into the test stands. Use the provided brushes to clean out each port.

- Purge the dry sand by going back to the “Manual Mode” screen and touching the red ON button (below blue button) and allow it to run out for 5 seconds. Press the same button again to shut it off.
- Use a ribbed aluminum rod to clear out the sand port while the emergency stop is activated. Do NOT put your hands in the chute.
- Turn the dial on the NexGen2 panel counterclockwise to the OFF position.
- Sweep up any sand mess and clean out the resin and catalyst test bucket by rinsing it with water. Return the kerosene to the flammable cabinet.

8.4 Appendix E: QCD-1 Specific Gravity and Porosity Measurement System SOP

- Fill the bowl with room temperature distilled water then place it on the lower platform (Figure E1).
- Attach the hanging platform to the suspension arm and let it rest in the water. The hanging platform should not touch the sides or bottom of the bowl.

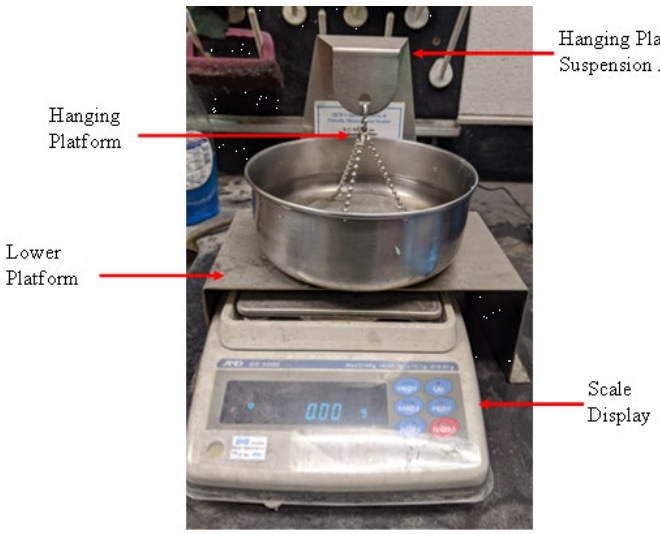

Figure E1. QCD-1 Specific Gravity and Porosity Measurement System (Q. C. Designs, Inc.)

- Turn on the scale using the button on the top left of the keypad. The scale should be zero-ed (Figure E2).

Figure E2. ASD GX-2000 scale display.

- Place the specimen on the hanging platform suspension arm. Wait for the mass reading to steady, then press the SAMPLE button (Figure E3).
- Move the specimen to the hanging platform. Ensure that the specimen is fully submerged and is not touching the bottom or sides of the bowl (Figure E3). Try not to splash any water.

Figure E3. The mass of the specimen noted in air (left) while resting on the suspension arm. The mass of the specimen fully submerged in water (right)

- Wait for the reading to steady, the press the SAMPLE button again. The density of the specimen will appear on the display in units of g/cm³.
- Press the SAMPLE button to clear any values and continue with measurements.

8.5 Appendix F: Brinell Hardness SOP

- Grind the sample surface until planar and all saw marks are removed. Clean and dry the surface.
- Set the specimen on the stage of the Brinell hardness indenter (Figure F1). Ensure that the proper indenter tip is inserted (10 mm).

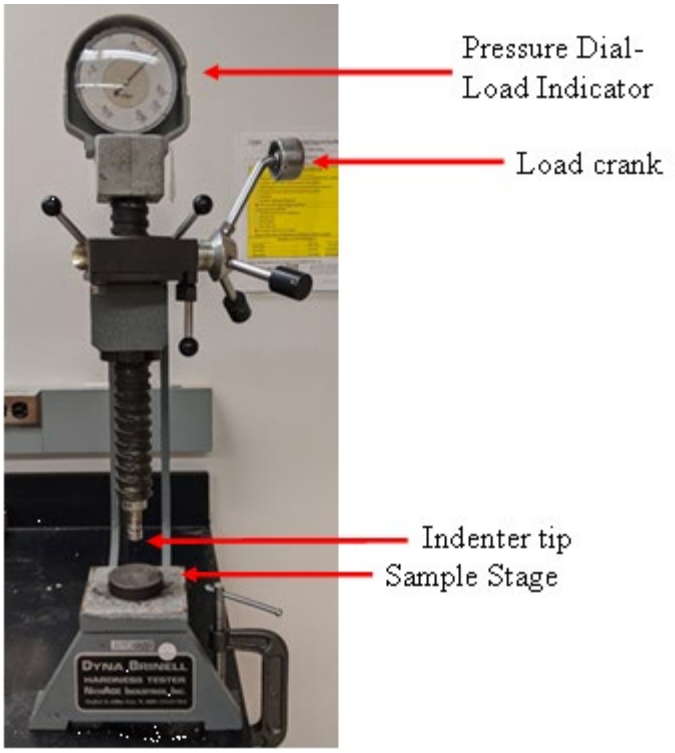

Figure F1. Dyna Brinell Hardness Indenter (NewAge Industries, Inc.)

- Lower the indenter tip to the surface of the specimen by turning the load crank clockwise. While holding the specimen still, continue to turn the load crank until the pressure dial reads the desired load (3000 kgf).
- Maintain the applied load for 15 seconds. Remove the load by rotating the load crank counterclockwise.
- Make 4 additional indentations following the above steps. Ensure that each indent is a minimum of two diameters away from the surrounding indentations.

- Using the Brinell Optical Scanning System camera, locate the first indentation. (Figure F2). Use the button to capture the indentation image and simultaneously measure the diameter and depth with the C.A.M.S. Testing System (Figure F2).

Figure F2. Brinell Optical Scanning System camera (NewAge Industries, Inc.)

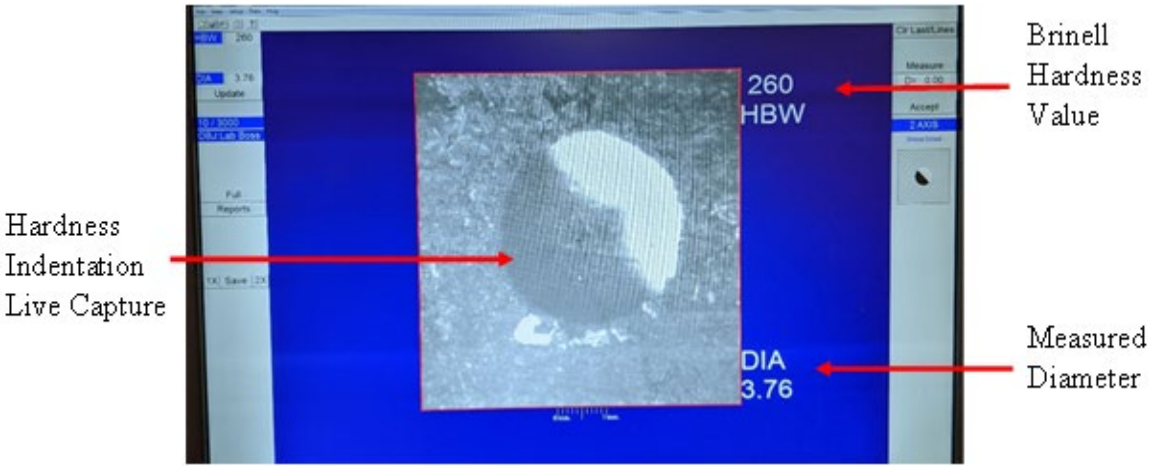

Figure F2. C.A.M.S. Testing System (NewAge Industries, Inc.) software with indentation live capture

- The Brinell hardness value and measured diameter will be displayed.
- Repeat with the remaining indentations, noting the values. They are not saved on the software.